2009-08-10

Design and Characterization of a Human Exposure Chamber and Inversion Episodes in Salt Lake City, Utah in January/February of 2009

Roman Yuri Kuprov
Brigham Young University - Provo

Design and Characterization of a Human Exposure Chamber and Inversion Episodes in Salt Lake City, Utah in January and February 2009

by

Roman Kuprov

A thesis submitted to the faculty of

Brigham Young University

in partial fulfillment of the requirements for the degree of

Master of Science

Department of Chemistry and Biochemistry

Brigham Young University

December 2009

BRIGHAM YOUNG UNIVERSITY

GRADUATE COMMITTEE APPROVAL

of a thesis submitted by

Roman Kuprov

This thesis has been read by each member of the following graduate committee and by majority vote has been found to be satisfactory.

Date	Jaron C. Hansen, Chair
Date	Lee D. Hansen
Date	Milton L. Lee

BRIGHAM YOUNG UNIVERSITY

As chair of the candidate's graduate committee, I have read the thesis of Roman Kuprov in its final form and have found that (1) its format, citations, and bibliographical style are consistent and acceptable and fulfill university and department style requirements; (2) its illustrative materials including figures, tables, and charts are in place; and (3) the final manuscript is satisfactory to the graduate committee and is ready for submission to the university library.

Date	Jaron C. Hansen, PhD Chair, Graduate Committee

Accepted for the Department

Date	David V. Dearden, PhD Graduate Coordinator

Accepted for the College

Date	Thomas W. Sederberg, PhD Associate Dean College of Physical and Mathematical Scienes

ABSTRACT

Design and Characterization of a Human Exposure Chamber

And

Inversion Episodes in Salt Lake City, UT

in January and February 2009.

Roman Kuprov

Department of Chemistry and Biochemistry

Master of Science

Research on health effects of particulate matter (PM) has been a very active area in the last two decades. One plausible mechanism by which exposure to PM affects human health includes modification of autonomic endothelium function. Decreased endothelium activity causes heightened risks of cardiovascular disease. A human exposure chamber designed to conduct experiments to quantify diminished function of endothelium from short term exposure to PM is described. The chamber consists of two stages for containment and pre-treatment of PM and exposure of human subjects. Concentrations of CO, CO_2, NO, NO_2, O_3, and $PM_{2.5}$, are monitored and

controlled in the exposure room. The PM used in the human exposure experiments was characterized chemically and morphologically.

During January and February of 2009, chemical analysis of $PM_{2.5}$ was done during inversion periods in Salt Lake City, UT. An Ambient Ion Monitor (AIM) was deployed to measure the concentrations of anions in both particulate and gas phases. The chemical data provided by AIM was complemented by measurements by the Department of Air Quality that included PM_{10}, $PM_{2.5}$, O_3, NO, NO_2, NH_3 and CO. The goal of the study was to determine whether ammonia or nitric acid is the limiting reagent in formation of PM during inversions. Nitric acid is the limiting reagent. Concentrations of ammonia are an order of magnitude higher than nitric acid.

ACKNOWLEDGEMENTS

First, I thank my adviser, Dr. Jaron Hansen, for his support, advice, and direction during my time as a graduate student as well as his example of work and dedication. Also, I thank Dr. Delbert J. Eatough for his patience and advice during my studies.

As my graduate committee member, I thank Dr. Milton Lee for his honesty humility, wisdom, and sincere care for my progress while in this program. I thank Dr. Arden C. Pope III for providing me with many insights into my studies as a graduate student but also as an example of humility and integrity in academic success.

I thank the faculty and staff of the Department of Chemistry and Biochemistry for being a friendly and a supportive bunch, these friendships and memories forged within the Benson building.

I thank Robert and Barbara Schwartz for their support, as they have been my family away from home, and I acknowledge and thank my mother for her incredible insight and encouragement.

Finally, I thank Heavenly Father for his loving, helping, and protecting hand throughout my life.

Contents

Chapter 1. Introduction

1.1 Introduction of PM

The most apparent indication of polluted air is reduced visibility, which is predominantly due to suspended particulate matter usually complemented by elevated NO_2 concentrations common in urban areas. [1]

Ambient particulate matter (PM) is composed of a wide range of species with various sources of origin, chemical compositions, and lifetimes. Such diversity is largely due to the abundance of chemical pathways and sources for creating and emitting PM into the environment. PM sources include combustion reactions, friction processes, bio-emissions from plants, animals, and humans, elevation and suspension of particles from the surface of the ground (during strong winds), condensation, and evaporation often observed in coastal areas. Sources emitting the PM directly into the environment are called *primary*, while *secondary* sources include the chemical pathways of forming PM from gases in the atmosphere. Secondary sources for PM formation include oxidation chemistry involving ozone, hydroxyl and hydroperoxy radicals and their higher derivatives, NO_2, SO_2, and various acid/base reactions involving NH_3, HCl, H_2SO_4, and HNO_3.

Particle diameters for particulate matter span five orders of magnitude, from 2 nm to 100 μm. The upper PM size range is typically composed of small ash fragments, plant spores, and fine sand and dust particles. The importance of these particles in the atmosphere is minimal due to their short lifetimes of several minutes brought upon by their fast sedimentation and washout rates. The smallest PM includes clusters of just a

few molecules. However, the exact threshold between a cluster of molecules and a particle is not clearly defined.

Although the term 'particulate matter' is used often and interchangeably with 'aerosol' there is a slight difference between the two definitions. While PM relates only to the particles suspended in air, aerosol definition includes both particles and the gas in which the particles are suspended.

1.2 Measurement and Characterization

Measurement and characterization of PM is hampered by several obstacles. The first major problem is the extremely large range of sizes that are classified as PM. A convenient way to classify PM is by the diameter of the particles. However, most particles in the troposphere are not spherical, and the particles emitted by different sources usually have different chemical compositions and densities, so their behavior in ambient air varies. Therefore, classification of particles is done by their aerodynamic or Stoke's diameters.

Aerodynamic diameter is defined as the diameter of a spherical particle with a density of 1 g/cm^3 that has the same settling velocity (terminal speed) as the particle in question. The advantage of this approach is that it describes a particle's mobility in the troposphere. The aerodynamic diameter is calculated as:

$$D_a = D_g k \sqrt{\frac{\rho_p}{\rho_0}} \qquad \text{(Eq. 1)}$$

where D_g is the geometric diameter, k is the shape factor (which equals 1 for a sphere and increases for more irregular shapes), ρ_p is the density of the particle, and ρ_0 is the

reference density of 1 g/cm^3. This method relates the aerodynamic diameter to the density of a given particle. However, the density of particles is usually lower than that of their composing materials due to the presence of pores, cracks and other irregularities. Therefore, particles of high densities (more than 10 g/cm^3) are uncommon and the difference in aerodynamic diameter induced by the difference in particle densities usually does not exceed a factor of 4. Aerodynamic diameter is more useful for describing the behavior of PM in air as well as in the respiratory system. In this work, any reference to particle diameter is the aerodynamic diameter.

Stoke's diameter is defined as the diameter of a spherical particle that has the same density and terminal falling speed in air as the particle of interest. The relationship between Stoke's and aerodynamic diameter is expressed as:

$$D_a = D_s \sqrt{\frac{\rho \cdot C_s}{C_a}} \qquad \text{(Eq. 2)}$$

where D_s is the Stoke's diameter and C_s and C_a are the Cunningham slip factors evaluated for the two diameters respectively, while ρ is the particle density. The slip factor is a function of the ratio of the particle's diameter and the mean free path of the gas in which the particle is suspended. This mean free path is approximately 0.066 μm for air at 20 °C and 1 atm. Thus, for particles below 0.5 μm the slip factor becomes important since representing the suspension gas as a continuum becomes unreliable.

Another difficulty in particle measurement and characterization is a consequence of different particle compositions. PM can be classified as non-volatile and semi-volatile.

Non-volatile PM consists primarily of black carbon (soot) and oxides and salts of metals. Dust particles, plant spores, and fine sand particles also contribute to the non-volatile portion of ambient particulate matter.

Ammonium nitrate is a major components of semi-volatile PM produced via the reaction of gaseous nitric and ammonia (two of the most abundant species in the lower troposphere). Semi-volatile PM also contains a myriad of organic compounds that have relatively low vapor pressures. The low vapor pressure of these compounds allows their condensation and nucleation into particles at lower temperatures and evaporation at higher temperatures. Thus, the total PM in the troposphere can fluctuate with temperature.

Design and operation of analytical equipment requires consideration of the size distribution range and particle physical properties. Collection temperatures and pressures must be taken into account to obtain meaningful data.

Sampling of non-volatile PM is relatively straightforward and is frequently accomplished by filtration devices. An example of such an instrument using this approach is a TEOM (Tempered Element Oscillating Microbalance) which collects the non-volatile PM on the surface of a small quartz filter at a given temperature and oscillating at a certain frequency. Accumulation of PM mass on the filter decreases its oscillation frequency which is translated and reported as the mass of collected material. Another instrument using a filtering technique for measurement of non-volatile PM is an Aethelometer. The Aethelometer introduces a flow of sample air through a quartz filtration tape while measuring the attenuation of both an IR and UV beam directed through the tape. The difference in beam intensity is converted into the mass of collected PM.

Semi-volatile organic matter is usually measured via one of two methods. The first involves collection with an organic sorbent material (such as activated carbon), followed by analysis of collected material. This method may require prior removal of

non-volatile PM matter from the sample air stream. Final analysis of the collected semi-volatile PM can be performed by a variety of analytical methods, including HPLC, MS, and temperature volatilization. The second method relies on the difference between the particle mass collected at two different temperatures, typically 50 °C and 4 °C . This method assumes that the semi-volatile PM collected at low-temperature is evaporated at high-temperature, and the difference between the two reported values is the measure of the semi-volatile component. An example of such an instrument is an FDMS-TEOM (Flow Dynamics Measurement System – Tempered Element Oscillating Microbalance).

Particle selection is usually done by means of cyclones, impactors, electrostatic precipitators, or filters (filters being less common). The goal of these devices is to let a certain range of particle sizes through while prohibiting the rest from entering the instrument. Impactors and cyclones use the same principle which is based on particles with sufficient inertia continuing along their original flight path when the air stream abruptly changes direction, forcing deposition of larger particles on the walls of the device. This method allows setting an upper size limit and permitting passage only of particles below that size. A basic diagram of a sharp cut cyclone is presented in Figure 1.

In an electrostatic precipitator, particles are passed over a charge inducing element (usually a radioactive material) that imparts an electric charge to a particle. The stream of charged particles is then directed down a selection chamber with walls of a controlled electric potential. Particles of low aerodynamic diameter to charge ratio (D_a/z) deposit onto the walls of the selection chamber and those of higher D_a/z pass into the

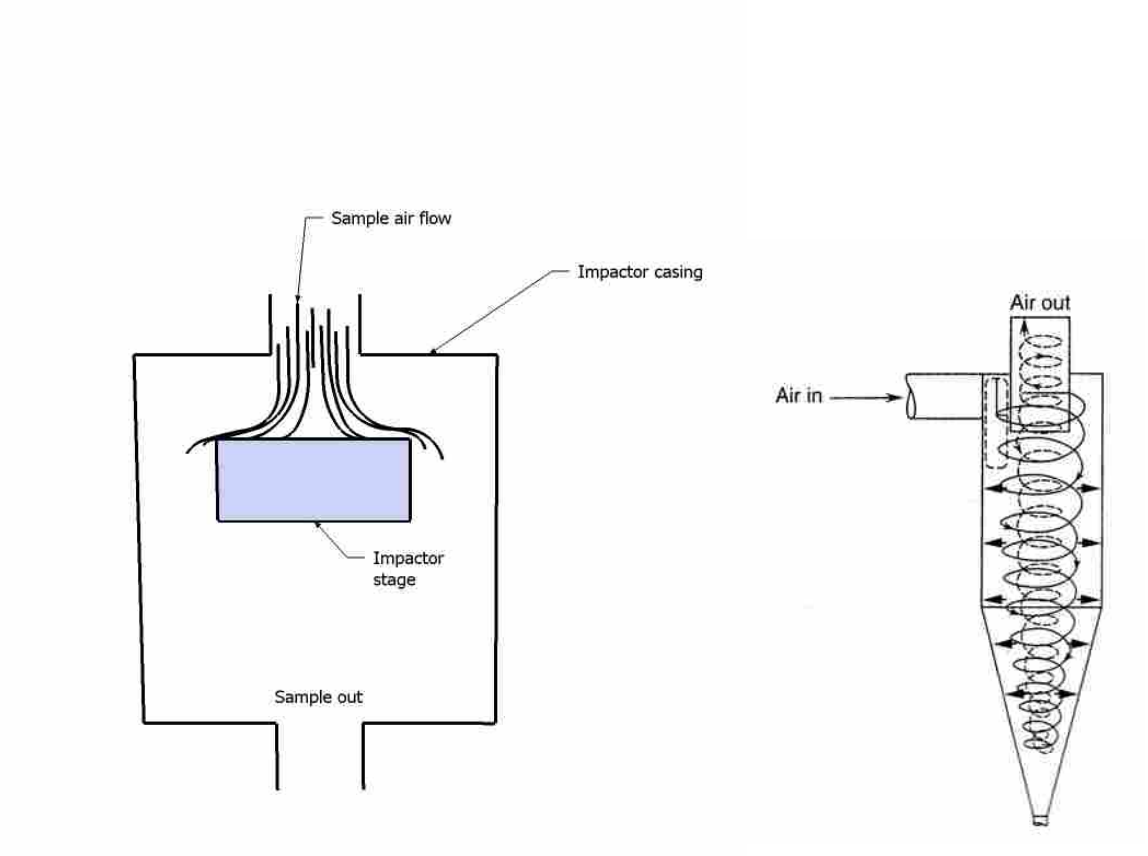

Figure 1. A scheme of a typical impactor and a cyclone. A sample stream entering the impactor is redirected abruptly by the impactor stage. A sample air stream enters the cyclone and is forced to spiral downwards. Particles with larger aerodynamic diameter deposit on the walls while small particles continue along with the air flow.

detection mechanism. Electrostatic precipitators also allow quick and accurate scanning of PM sizes.

Size characterization of PM is defined by a 50% cutoff of the desired size.[2] The 50% cutoff is equal to the diameter of spheres of 1 g/cm^3 density which are collected with 50% efficiency. Thus, assuming that a sample air stream contained PM no larger than 20 μm was directed through an impactor stage with a 50% cutoff point of 8 μm, it would collect 14 μm – 6 μm particles.

1.3 Mass, Size, Mode Distribution and Sources of PM

Suspended particulate matter in the air is present in three distinct modes: coarse, accumulation, and transient or Aitken nuclei.[3] A fourth mode, ultra-fine, is generally accepted as PM with an aerodynamic diameter less than 0.01 μm, although there is no universal agreement as to the definition of ultra-fine particles.

The trimodal distribution of PM is related to the sources of particles in each mode. A representative diagram of this modal size distribution is displayed in Figure 2.

Particles with aerodynamic diameters above 2.5 μm are considered to be in the coarse particle range. Particles in the coarse mode comprise a significant fraction of the total ambient PM by mass, but only a very small portion of the total population. These particles are mostly produced by mechanical processes, such as friction and grinding, but can be biogenic in nature; i.e., spores and pollen.

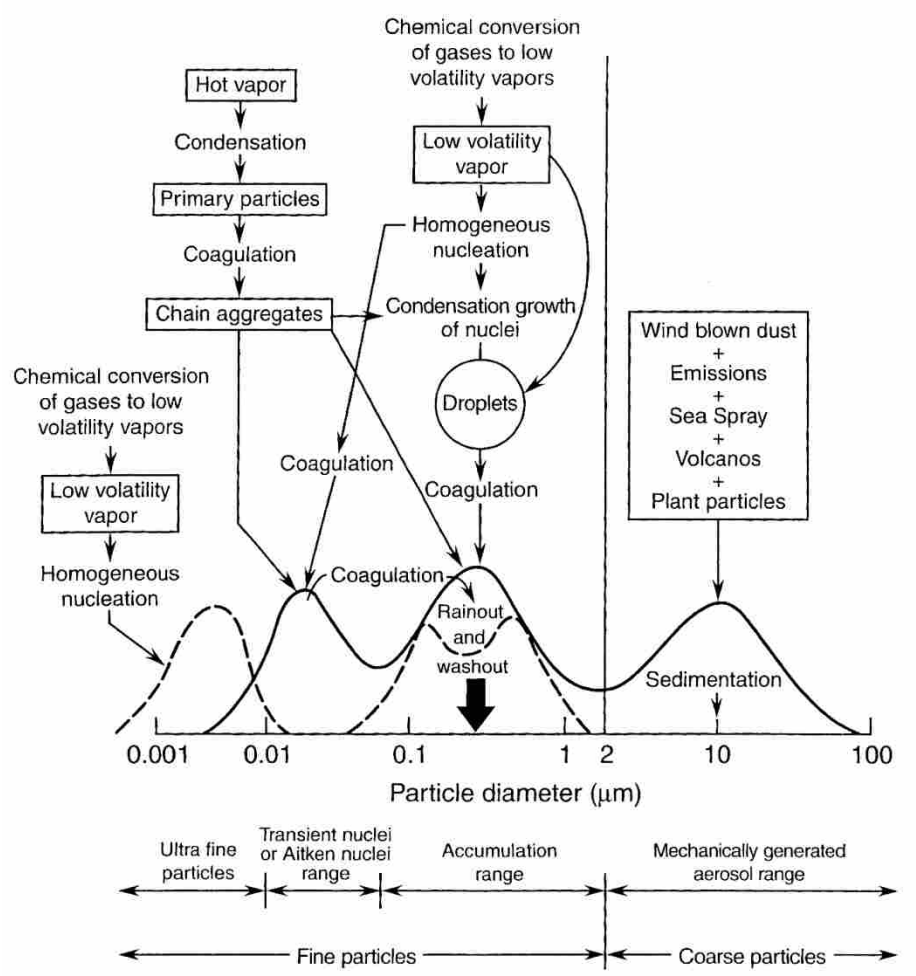

Figure 2. The three major modes are outlined by the solid line. The ultra-fine particles as well as the double peak feature of the accumulation mode are presented by the dashed line. Formation sources as well as the removal mechanisms (sinks) and their interrelation is also displayed. (Adapted from Finlayson-Pitts and Pitts, 2000, p. 355)

Particles entrained from the surface of the ground by wind, such as fine sand, also fall into the coarse range. It would be incorrect, however, to assume that all mechanical or meteorological processes produce particles only in the coarse mode as they may emit a wide range of particles.

The chemical composition of coarse particles generally represents their source. Particles lifted off the surface of the ground will have a predominantly crustal material composition, while those produced by grinding or erosion will contain the substances from the bulk material from which they originated, most commonly inorganic salts.

The rapid gravitational settling and washout of coarse particles makes them less important in atmospheric processes. However, during some meteorological processes, such as sand storms, these particles may obtain an electrical charge which negates their gravitational settling and reinforces reentrainment.[4] Under such condition, coarse particles may be carried over significant distances and may be an important method for transport of pollution. Coarse particles have been observed to traverse the Atlantic from Africa to the Americas.[5-8]

Particles in the size range between 0.1 μm and 2 μm are defined as the accumulation range. The chemical composition of these particles does not generally reflect their origin as clearly do coarse particles. Accumulation particles occur as the product of combustion processes as well as from condensation of low volatility vapors. Accumulation particles contain a larger measure of organic compounds than coarse particles, primarily due to condensation processes. Particles in the accumulation range primarily grow through collisions with smaller particles in the nucleation mode and the lower end of the accumulation range. Because of their larger surface area and lower

mobility, larger particles in the accumulation range tend to grow faster through such collisions than smaller particles. Additional accumulation particle growth pathways include heterogeneous oxidative chemistry, e.g. conversion of SO_2 to SO_4^{2-}, direct condensation of low vapor pressure species, and uptake of water from the air.

Accumulation range particles constitute the smallest portion of the total particle number but represent a significant (up to 50%) fraction of the total PM mass. This is primarily due to the longevity of the particles in the air caused by their very slow fallout rate of a few hours. The two primary removal mechanisms for these particles are washout through precipitation and incorporation of the particles into water droplets of fog or clouds. Thus, depending on the meteorological conditions, accumulation range particles can persist in the air for a significant period of time, up to several hours.

Particles in the accumulation range are primarily responsible for the visibility loss during daytime. Their effects on human health and visibility make the accumulation range particles a significant factor in atmospheric chemistry research as well as public health and regulation.[1, 9]

Aitken nuclei particles are those with aerodynamic diameters between 0.1 and 0.01 μm. These particles have their origin in high temperature combustion processes and gas-to-particle formation mechanisms. The lifetimes of Aitken nuclei particles are very short, no more than a few minutes, due to their coagulation (between themselves or with particles in the larger size modes) and fast growth towards the accumulation range. These particles also serve as nuclei for condensation of low vapor pressure substances. Although these particles constitute the majority of the total number of the particles in the air, they contribute only a small portion to the total weight of PM due to their small sizes.

The fourth mode, ultra-fine particles or nucleation mode, is formed by gas-to-particle formation processes. The mechanisms driving the formation are not yet well understood.

1.4 Health Effects of Particulate Matter

Understanding of the effects of airborne particulates on human health began in the early part of the nineteenth century. The early pollution-to-health associations were made during remarkable and singular air pollution episodes in Europe.

One of the most prominent events that linked high particulate matter pollution with mortality happened in the Meuse Valley in Belgium in 1930. The valley, situated around the Meuse River and surrounded by elevated grounds, was rich with various factories, smelters, steelworks, fertilizer plants and other industrial establishments. In December, a thick fog settled over the area. During several days of air entrapment, large numbers of valley residents experienced severe respiratory symptoms. By the end of the episode, upwards of sixty individuals were dead. Later, this event was named the Meuse Valley Disaster.[10]

Another, arguably the most prominent, pollution episode happened in London in December 1952, when, due to unusually cold temperatures, coal burning emissions from house warming stoves reached an all time high. Coupled with the emissions from power plants and motionless air, a thick fog covered the city. During the following week, death rates within the city reached 900 per day totaling over 4,000 deaths attributed to the smog episode at the end of its five day length. Those having prior or chronic cardiac or

pulmonary conditions were at high risk for complications or death. Death rates remained elevated throughout the following year.[11, 12]

Although the connection between increased PM pollution and mortality was generally established, interest in research in the health effects of PM did not spike until the early 1990's. The terms $PM_{2.5}$ and PM_{10} were coined as PM characterizations relevant in human studies. $PM_{2.5}$ refers to particles with the aerodynamic diameter <2.5 μm, while those with diameter <10 μm are referred to as PM_{10}.[2] In the United States, public policy establishing permissible levels of PM is directed towards regulating $PM_{2.5}$. This is justified because $PM_{2.5}$ is small enough to penetrate deep into the thoracic region and stay longer in the suspended state. Additionally, the toxicity of $PM_{2.5}$ may be increased due to its higher surface-to-mass ratio when compared with PM_{10}.

Several studies conducted in Utah Valley in the early 1990's as well as the Harvard Six Cities study pioneered research connecting PM to human health.[13] The association between PM and hospital admissions, respiratory symptoms, school absences, and mortality were established in Utah Valley studies.[14-16] At the same time, the Harvard Six Cities study connected cardiopulmonary mortality in adults and respiratory symptoms in children to elevated PM concentrations, effectively jump starting research on PM effects on human health. Although cause-effect of PM pollution and the increase in cardiopulmonary symptoms and mortality was established, the exact mechanism by which PM undermines human health is not clearly understood.

One of the mechanisms by which PM is hypothesized to present a health threat is by exacerbation and accelerating Chronic Obstructive Pulmonary Disease (COPD). Studies conducted by Avol et al. and Gauderman et al. showed a significant decrease in

the lung capacity of adolescent children living in areas with elevated air pollution.[17, 18] Individuals developing chronic cough, bronchitis, and decreased lung function when exposed to long-term PM pollution reaffirmed this hypothesis.[19-23] However, acceleration of COPD could not account for the increase in cardiac symptoms during the pollution episodes. One of the links between COPD and elevated cardiac risks was identified by van Eeden et al. as systemic inflammation.[24]

Another proposed mechanism for PM health effects included systemic and pulmonary oxidative stress, inflammation, and progression of atherosclerosis.[25] Exacerbation of lung disease, increased blood coagulation, and alveolar inflammation could also account for increased cardiovascular cases of mortality during high PM episodes.[26] Two separate studies by Souza et al. and Schwartz et al. associated exposure to PM with increase in blood markers linked with cardiovascular risk: fibrogen levels, white blood cell count, and platelets, as well as chronic inflammation and lung injury.[27, 28]

PM exposure has also been associated with the change in cardiac autonomic function. Although the physiologic significance of heart rate variability (HRV) is not well understood, it was shown to be related to cardiovascular mortality risk.[29, 30] Several animal studies have linked the change in HRV to exposure to PM.[31-33] In a very insightful experiment, Schwartz et al. linked the oxidative stress caused by the exposure to PM to variations in HRV.[34] The group observed the effects of PM exposure on individuals with absent allele for glutathione S-transferase M1 (GSTM1) that encodes for an enzyme scavenging reactive oxygen species. The change in HRV in the subjects without GSTM1 was not observed in the individuals who had the allele. The results suggested that some of

the systemic inflammation caused by inhaled PM occurs via reactive oxygen species and can be mitigated by antioxidants, e.g. statins, ibuprofen, fish oil.

Another mechanism by which PM increases the risk of cardiovascular failure is the activation of endothelium. Endothelium is the innermost layer of cells covering the blood vessels. It controls the autonomic expansion and contraction of the vessels. Brook et al. showed that exposure of healthy adults to PM and ozone induced vasoconstriction of brachial artery.[35] However, arterial vasoconstriction cannot be viewed independently of the previously described mechanisms because of its relation to the systemic inflammation due to the oxidative stress, COPD induced inflammation, and atherosclerosis related pathways.

Other pathways to induce cardiovascular risk may include the translocation of ultra-fine particles through the respiratory system directly into the blood, as was shown in hamsters[36] and humans[37], decrease in immune response[38], and PM induced lung damage[39].

A more detailed and thorough discussion of health effects of PM can be found in a review published by Pope and Dockery in 2006.[9]

1.5 National Ambient Air Quality Standards

Due to the importance of PM_{10} and $PM_{2.5}$ in public health and visibility, the EPA considers PM a harmful pollutant. PM_{10} and $PM_{2.5}$ are strictly regulated along with the other principal pollutants. The highest permissible values to ensure the safety of public health including special groups (such as asthmatics, children, and the elderly) are called primary standards. Secondary standards reflect the highest permissible concentrations of

the principal pollutants to protect public welfare, animal life, vegetation, public and private property, etc. The primary and secondary standards for principal pollutants are shown in Table 1.

Areas that fail to comply with the Primary National Ambient Air Quality Standards (NAAQS) are deemed as unattainment areas, and as such have 5 years to provide a reasonable plan to bring pollutants below the NAAQS levels. Failure to comply results in severe cutbacks of federal funding.

1.6 Research Goals and Motivations

Two separate research efforts are presented in the current work. The first, in collaboration with Dr. Arden Pope III, measured endothelial function in adults with controlled exposure to PM from combustion of coal and wood. This part of the project is reported elsewhere. The part of the project described here was to construct an exposure facility that allowed controlled and safe exposure of human subjects to known concentrations of PM and chemical and physical characterization of the PM generated during the exposure experiments.

The second research effort was conducted with and sponsored by the Utah Department of Air Quality during January and February of 2009 in the Salt Lake valley. The primary goal of the study was to determine the chemical composition of $PM_{2.5}$ during inversion episodes common during winters and assist with the formation of a strategy to decrease the formation of PM pollution.

National Ambient Air Quality Standards

	Primary Standards		Secondary Standards	
Pollutant	**Level**	**Averaging Time**	**Level**	**Averaging Time**
Carbon Monoxide	9 ppm (10 mg/m^3)	8-hour	None	
	35 ppm (40 mg/m^3)	1-hour		
Lead	0.15 $\mu g/m^3$	Rolling 3-Month Average	Same as Primary	
	1.5 $\mu g/m^3$	Quarterly Average	Same as Primary	
Nitrogen Dioxide	0.053 ppm (100 $\mu g/m^3$)	Annual (Arithmetic Mean)	Same as Primary	
Particulate Matter (PM_{10})	150 $\mu g/m^3$	24-hour	Same as Primary	
Particulate Matter ($PM_{2.5}$)	15.0 $\mu g/m^3$	Annual (Arithmetic Mean)	Same as Primary	
	35 $\mu g/m^3$	24-hour	Same as Primary	
Ozone	0.075 ppm (2008 std)	8-hour	Same as Primary	
	0.08 ppm (1997 std)	8-hour	Same as Primary	
	0.12 ppm	1-hour (Applies only in limited areas)	Same as Primary	
Sulfur Dioxide	0.03 ppm	Annual (Arithmetic Mean)	0.5 ppm (1300 $\mu g/m^3$)	3-hour
	0.14 ppm	24-hour		

Table 1. Primary and secondary standards for principal air pollutants set by EPA as of 2008. (adapted from www.epa.gov/air)

Chapter 2. Human Exposure Chamber Design and Characterization

2.1 Introduction

The most frequent cause of death among adults in the United States is disease of the heart (principally heart attacks), followed by cancer, and cerebrovascular diseases (stroke).[40] Two of the three main causes are related to the function of the cardiovascular system. As discussed before, long term exposure to elevated levels of particulate matter (PM) pollution have been implicated in the increased risk of the onset of ischemic heart disease and sub-clinical chronic inflammatory lung injury and atherosclerosis. A proposed mechanism for the effects of PM exposure on the cardiovascular system is via an inflammatory response of the endothelium.

Although the effects of exposure to ambient pollution in humans have been studied, and the effects of exposure of experimental animals to concentrated ambient particulate material CAPS has been reported in several studies, a study of the effects of direct, short-term exposure of humans to PM in laboratory conditions have not yet been performed.[41-43]

Several designs for controlled human exposure to gases and PM have been developed. These include full-body exposure chambers, hoods, and masks.[44-46] Particulate matter generation in these systems employs either on-board production of pollution via previously obtained powder samples (wheat flour, dust, etc.) or the use of the particulate pollution directly extracted and concentrated from ambient atmospheric conditions.

This chapter describes the design and performance of a two-stage PM exposure chamber for human subjects developed to study the effects of short-term PM exposure. The design of this chamber allows: 1) a near-real time monitoring of the concentrations of non-volatile and semi-volatile PM, 2) measurement of the time-dependant size distribution, and 3) the concentrations of CO, CO_2, NO_x, and O_3. The current design allowed pretreatment of PM prior to human exposure. During this study PM was photochemically aged via exposure to UV radiation to further simulate daytime tropospheric conditions.

2.2 Exposure Facility Design

Wood and coal were used as fuels for the generation of particulate matter. Six volunteer subjects were exposed to 175-200 $\mu g/m^3$ PM from combustion of coal or photochemically aged wood for three hours. Coal and wood were used as fuels for particle generation in part because of their universal use and because the chemical composition of PM generated during their combustion is different. Figure 3 shows a schematic of the exposure room and PM/gas conditioning system. The exposure facility is comprised of two separate compartments: a ~30 m^3 Teflon bag and the ~ 14 m^3 exposure room. The Teflon bag is designed to contain the source PM during an experiment and photochemical pretreatment of the PM is done in the bag.

The bag is constructed of 0.3 mm thick Teflon film, heat-sealed with a Vertrod sealing blade iron. A 3 inch wide (7.5 cm) adhesive polysilicone tape (R.S. Hughes Co. Inc., p#8403) was laid over each seam to provide additional structural integrity and shape to the bag. Teflon film was used because of Teflon's chemical inertness and high

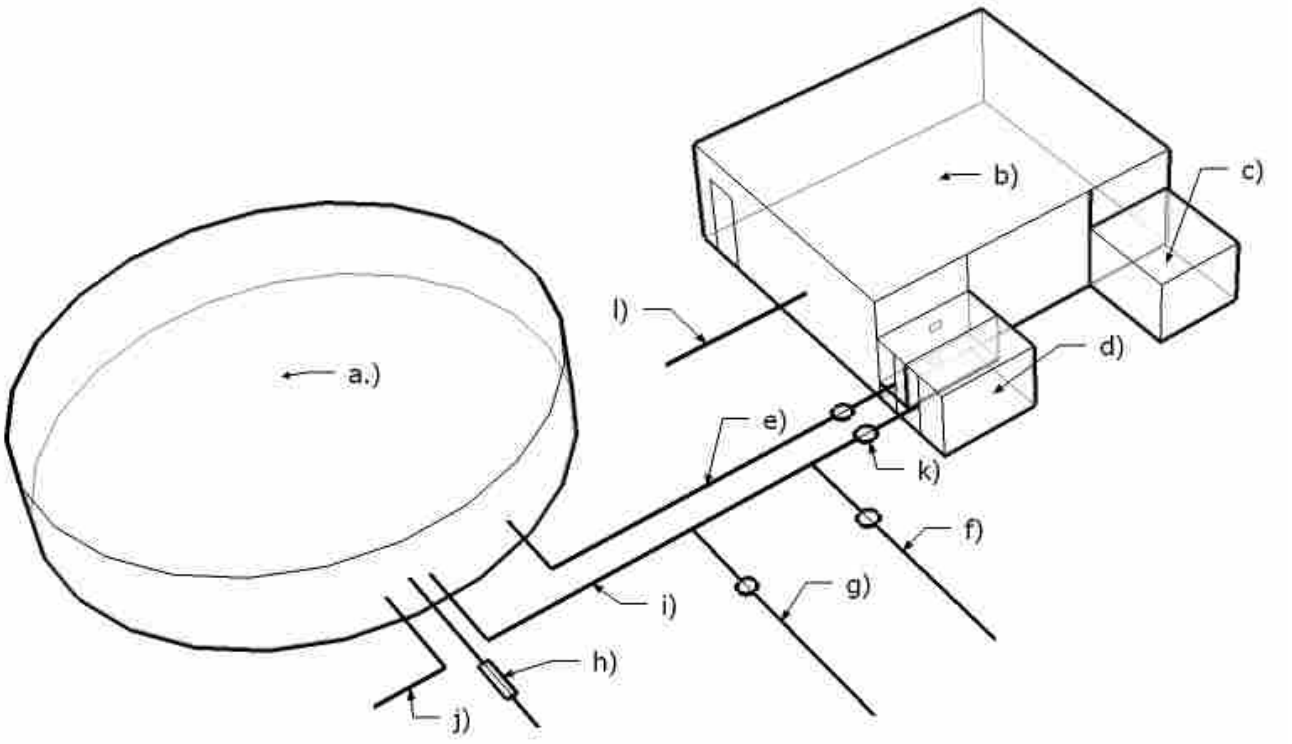

Figure 3. Diagram of the Human Exposure Chamber. a) Teflon bag; b) human exposure chamber; c) internal air circulation pump; d) bag-chamber transfer pump; e) bag-to-chamber transfer line f) bag purge line; g) filling line; h) particle intake line and catalyst; i) chamber-to-bag transfer line; j,k) chamber and bag sampling manifolds; UV lights not shown.

transmission of UV radiation which is used to photochemically age the PM inside the bag.

A utility manifold at the bottom of the Teflon bag allows instrumentation interface as well as air and particle delivery. Sampling tubes that enter the bag via a Teflon manifold are either stainless steel or Teflon to decrease reactivity with the contents.

Additionally, an in-bag fan with Teflon coated blades extends through the manifold to gently stir the contents of the bag. 40-50 rpm provided acceptable mixing of the PM inside the bag. Higher rotation speeds resulted in increased particle deposition to the walls of the bag.

To simulate photochemical atmospheric conditions, a set of 200 F40BL GE black lights (maximum output at 365 nm, irradiance of 0.28 $W/m^2/nm$) and 12 FS40UVB (maximum output at 312 nm, irradiance of 0.38 $W/m^2/nm$) lamps from Commercial Lighting (SLC, UT) were placed above the Teflon bag. To ensure homogeneous light distribution, the lamps were set 3 inches (7.2 cm) apart from each other and distributed across the ceiling above the bag.

A ~14 m^3 exposure room was located below the Teflon bag. Accommodations within the exposure room included a small sofa, four chairs, a small desk, and a small refrigerator. The room was isolated from the building's ventilation system to avoid unnecessary loss and dilution of the PM. To avoid loss of PM when subjects' entered and exited the room, two layers of heavy Teflon film were fastened to the door frame to create a veil with overlapping flaps. This significantly reduced the amount of PM dissipated into the areas outside the exposure room when opening and closing the door. With the door open, gases may disperse between the flaps of the Teflon strips into the

outside area, but the majority of PM is retained. This provided a mechanism whereby the gas phase concentrations of NO, NO_2, CO, CO_2 and O_3 could be lowered while at the same time maintaining the PM concentration in the exposure room.

An internal circulation blower with a pumping capacity of ~ 1 m^3/min was attached to the exposure room to provide circulation and a homogeneous mixing of PM in the exposure room. To ensure a homogeneous mixture, the internal circulation vents were placed opposite each other near the floor and the ceiling of the room. The blower was operated at all times during the human exposure experiments. Although the constant motion of PM through the air circulation system increased the PM loss to the walls of the room, this disadvantage was necessary to maintain a homogeneous PM mixture in the exposure room.

The room and the Teflon bag were connected via two 2-inch (~5 cm) diameter PVC transfer pipes with a valve system through which the delivery of PM into the exposure room could be controlled. The pipes were connected directly into the bag through the Teflon manifold. A transfer blower facilitated the exchange of air from the Teflon bag into the exposure room. Tubing for emptying and filling the bag was attached to the transfer pipes, which allowed for the option of filling the bag during exposure experiments while maintaining the PM concentration in the room relatively constant.

2.3 Particle Concentration Control and Transfer

Prior to the start of an exposure experiment, the bag was filled with dry, filtered laboratory air. The particulate matter was generated by burning coal or wood in a

Regency™ wood burning stove, see Figure 4. At least 15 minutes of a steady rate of burning was allowed before PM was directed from the smoke stack into the Teflon bag. When burning wood, a slightly opened oven door provided sufficient air flow to maintain a steady combustion rate. In the case of coal, additional air flow was provided into the stove via an air tube inserted through the bottom of the stove to facilitate a more complete and steady combustion. Coal combustion temperatures were estimated visually. Relatively high combustion temperatures (>600°C for wood and >1000°C for coal) were required for production of smaller size particulate matter as well as a more complete decomposition of long-chain hydrocarbons. Lower combustion temperatures (<500°C and <800°C for wood and coal respectively) resulted in quick failure of the TEOM and FDMS-TEOM due to rapid deposition of char on the microbalance filters which prohibited air flow through the instrument. This was avoided at higher burn temperatures. If photochemically aged PM was to be generated, the UV-black lights were turned on at the time of infusion of the wood smoke into the bag and remained on for the duration of the experiment. The wood smoke was considered photochemically aged after an hour of UV exposure.

After 15 minutes of steady combustion, the PM was transferred into the Teflon bag through a 2.5cm diameter steel tube attached to the stove smoke stack. A squirrel cage blower was used to transfer PM into the bag. Prior to entering the bag, the air

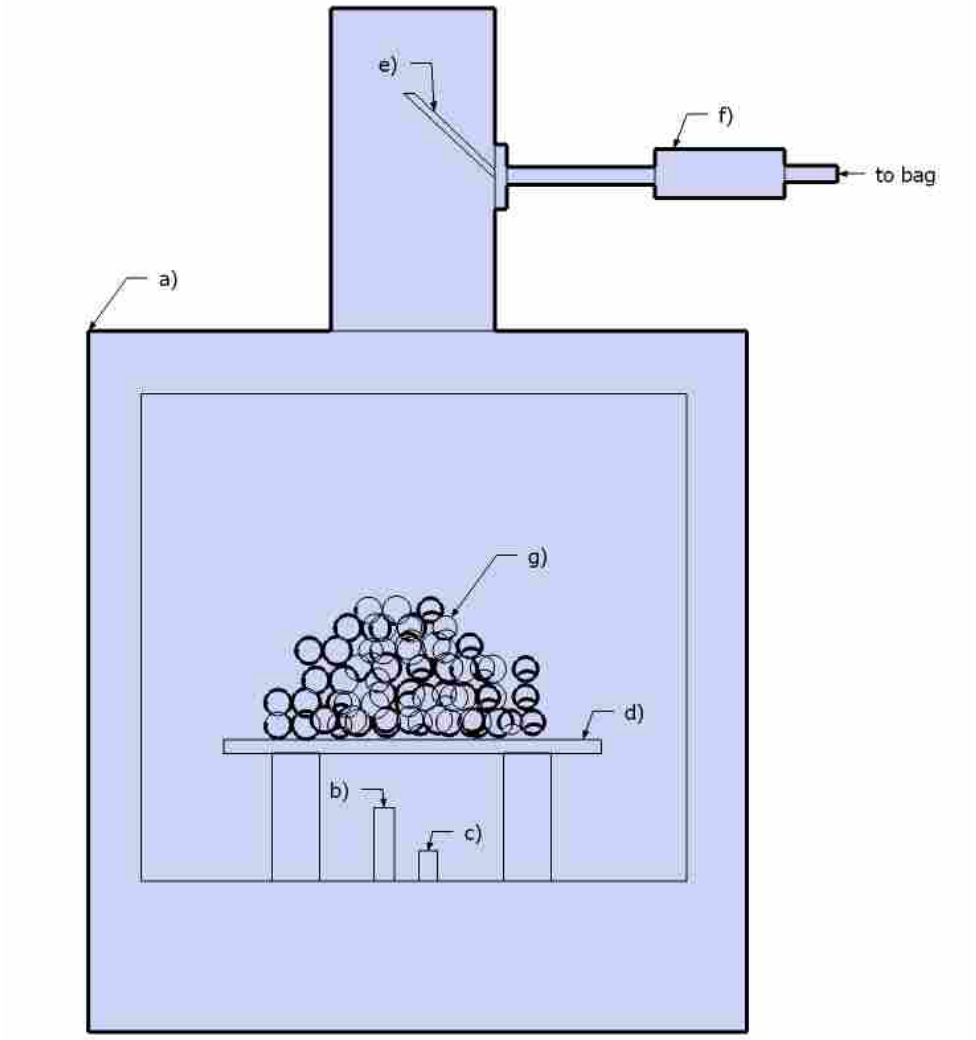

Figure 4. Oven setup for burning coal. a) Oven; b) Bunsen burner; c) air supply tube; d) stainless steel mesh; e) PM intake tube; f) catalyst enclosure; g) coal.

containing PM was passed over a ceramic honeycomb, Au-doped catalyst heated to 85-90˚C. The catalyst converts CO into CO_2 with nearly 95% efficiency with minimal loss of PM.

Transfer of PM from the bag into the room was done through a high-volume transfer blower attached to the side of the exposure room. The blower transfers the room air into the bag through one of the transfer pipes, creating a pressure differential between the bag and the room. The second transfer pipe is opened to allow transfer of the Teflon bag contents into the exposure room. A small fan was installed in the ventilation orifice on the exposure room side to aid in the transfer of the PM from the bag.

FDMS-TEOM (R&P Model 8400) and TEOM (R&P Model 1400a) monitors were attached to the bag manifold to monitor the concentration of total and non-volatile PM, respectively. To keep the PM concentration inside the exposure room within the desired value (175-200 $\mu g/m^3$), the PM concentration inside the bag needed to be about 1200 $\mu g/m^3$. Concentrations higher than 1800 $\mu g/m^3$ inside the Teflon bag caused rapid microbalance filter overload in the FDMS-TEOM and TEOM. Running 10 minute averages of the PM concentration in the room was recorded every 10 seconds by the TEOM instrument (filter temperature was set to 30˚C, main flow 3.00 lpm, auxiliary flow 13.64 lpm). A running 15 minute average of semi-volatile and non-volatile PM in the bag and room was recorded with FDMS-TEOM every 15 minutes (filter temperature at 30˚C, main flow 3.00 lpm, auxiliary flow 13.64 lpm). To monitor the PM aerodynamic diameter size distribution, a suite of TSI instruments, including a Scanning Mobility Particle Sizer (SMPS 3936), Electrostatic Classifier (EC 3080), and Concentration

Particle Counter (CPC 3022A) was used (sample flow 0.13 lpm, sheath flow 1.3 lpm). Particle size distribution data was collected at five minute intervals.

The conditions in the exposure room were monitored through a stainless steel manifold internally coated with Teflon. The manifold was attached to a 1 inch diameter stainless steel pipe (approximately 1 m in length) that was inserted into the exposure room. The manifold allowed for attachment of another set of TEOM and FDMS-TEOM instruments, CO (Thermo Inc., Model 42), NO, NO_x (Thermo Inc, Model 48), and O_3 (Dasibi Env. Corp., Model 1003-PC) concentration meters, and a set of three filter packs (a 47mm, 0.2 μm Teflon filter (Whatman), a 0.4 μm Nucleopore filter (Whatman), and a 47 mm prefired quartz filter (GelmanSciences) followed by a 47 mm carbon impregnated filter, (GelmanSciences)). The levels of CO_2 were monitored via a handheld monitor (Telarie 7001) located in the exposure room. If gas concentrations within the exposure room rose sharply or began to exceed the predetermined experimental values, the door into the exposure room was opened to lower the gas concentrations with little to no particle loss. This method provided an efficient and quick way of controlling the gas concentrations within the room. The rate ($t_{1/2}$~15 minute) of PM decay inside the exposure room demanded periodic infusion of PM and gases from the Teflon bag into the room about every ten minutes. The concentration of PM in the exposure room was controlled by the time interval between and the duration of the infusion events.

2.4 Particle Size Distribution, Deposition and Coagulation

The lifetime of PM in the exposure room was determined by infusing the room with PM and monitoring the decay rate. Figure 5 displays the graph of normalized decay curves of the photochemically aged wood smoke and non-aged wood and coal smoke. Secondary production of PM due to the reactions attributed to photochemical aging was evidenced by the change in the decay order of the PM as well as the increase in the total particulate concentration. The decay rate of non-photochemically aged coal and wood smoke was determined to be first order (k_{wood} = -0.071 hr^{-1}, k_{coal} = -0.083 hr^{-1}); however, secondary particle formation during UV exposure of wood smoke shifted the decay rate to be neither first nor second order. Normalizing the PM concentrations during the decay studies and integrating with respect to time confirmed the secondary production of particulate matter in the wood smoke during UV exposure. The initial curvature of the photochemically aged wood smoke line as well as its elevated position in relation to the other graphs suggests secondary particle formation. Both non-aged coal and wood smoke decays fit well and behave as first order decays. It is important to notice that the decay curves shown in Figure 5 represent unperturbed decay of PM in the bag. Actual PM decay in the bag during the exposure experiments increased due to frequent addition of fresh air and mixing with less concentrated PM mixture from the exposure room.

PM in the exposure room was found to have a significantly faster decay rate than in the Teflon bag. This is due to the constant internal air circulation and the large, non-inert surface area of the objects in the room. Subjects entering and leaving the exposure room had little effect on the PM decay rate. However, the PM loss within the exposure room increased with the number of subjects present. Each six-hour exposure experiment

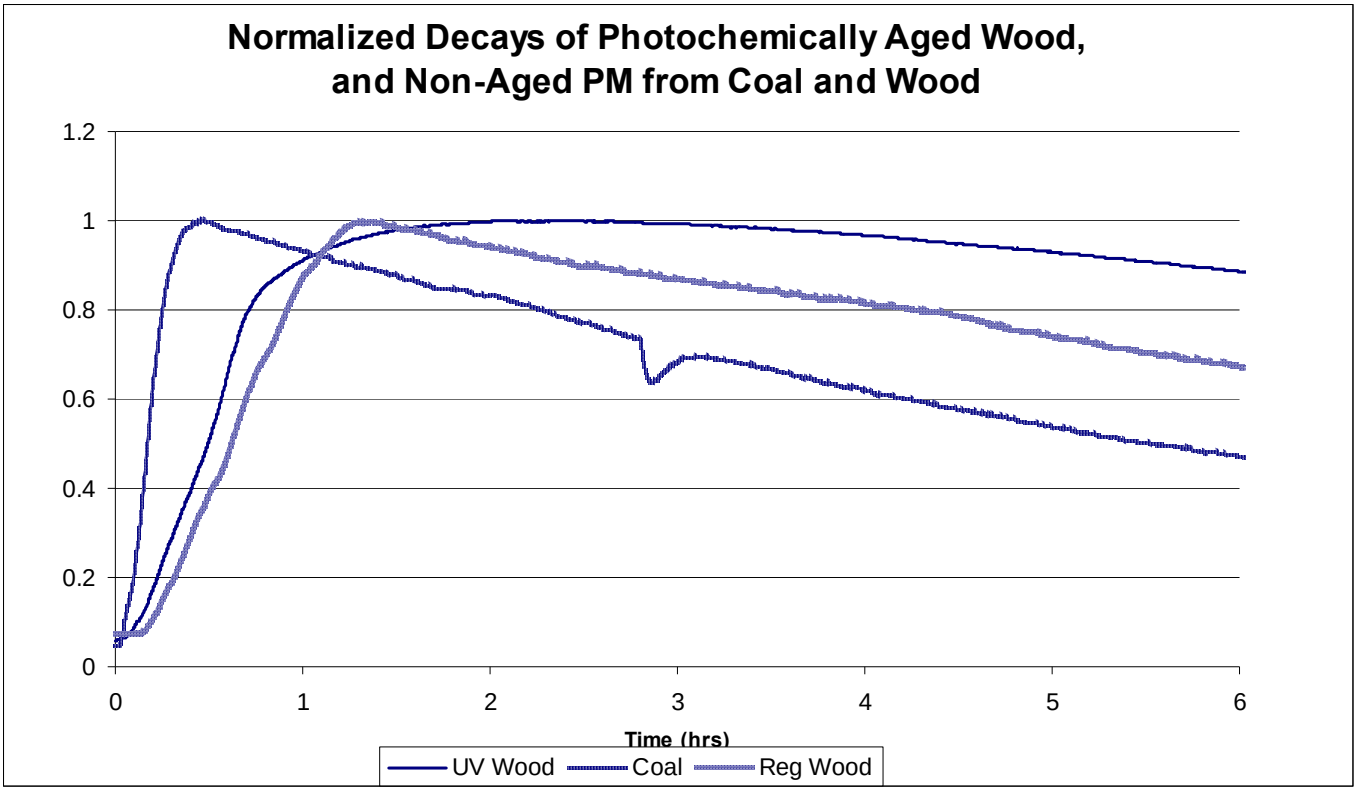

Figure 5. Normalized decay of wood smoke, coal smoke, and photochemically aged wood smoke. The apparent curvature and elevation of the photochemically aged wood smoke over the regular wood and coal smoke decay plots suggest secondary particle formation. The decay rates display particle decay in the unperturbed bag environment and do not represent the decays observed during the actual experiments.

involving human subjects required approximately eight additional PM infusions into the Teflon bag to keep the concentration above 1200 μg/m^3 when using coal. Because of the decreased decay rate and secondary particle formation two additions were needed for photochemically aged wood smoke.

As expected, at high combustion temperatures the majority of the particular matter produced was under 2.5 μm. This was confirmed by both scanning electron microscopy (SEM) images of the PM collected on a Nucleopore filter and the data collected by the TSI suite of instruments. Figure 6 shows SEM images of PM from coal and photochemically aged wood smoke. Particles from both coal and photochemically aged wood smoke collected on Nucleopore filters were mostly around 200 nm in diameter. PM from coal had a poorly defined, amorphous shape in contrast to the flakes of the photochemically aged wood smoke particles.

Freshly generated PM was predominately around 200 nm in aerodynamic diameter, but the mean particle diameter increased over time by particle accretion. In the case of photochemically aged wood smoke, the increase in particle diameter over time was more pronounced than in coal smoke due to secondary particle formation processes, see Figure 7. Secondary particle formation during photochemical aging of wood smoke was manifest by a decreased rate of loss of PM when compared to PM from coal. In the course of four hours, the decline in concentration for coal was nearly 80% of the original value, and only 30% for photochemically aged wood smoke. This disparity can not be attributed to the difference in aerodynamic diameter of wood and coal PM because the bulk of the PM was in the same ultra-fine range. Secondary formation of PM due to the

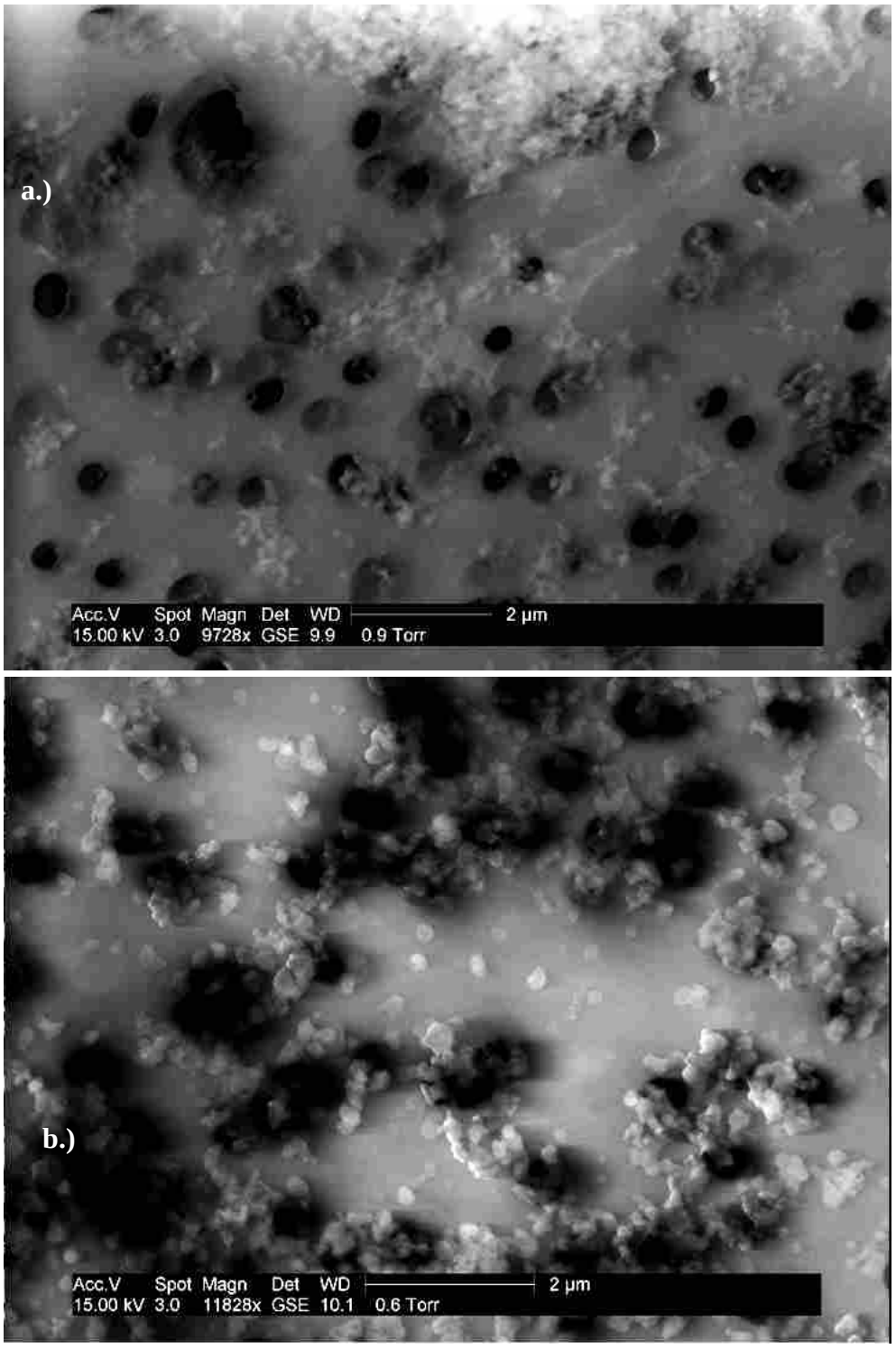

Figure 6. a) SEM image of coal smoke particles collected on a Nucleopore membrane filter. b) SEM image of wood smoke particles collected on a Nucleopore membrane filter. Both sets of particles are below 2.5 µm in size but have different textures.

reaction of photochemically created organic radicals and unburned hydrocarbons in wood smoke is a plausible explanation for the slower decay of the PM concentration of wood smoke in the bag.

2.5 Particle Composition

Coal and photochemically aged wood smoke particles were analyzed for anions with IC (ion chromatography). An IC3000 was used with an IonPac AS14A-5μm, 3x150mm analytical column produced by Dionex. The eluent was 8ppm $NaCO_3$, 1ppm $NaHCO_3$ aqueous solution. Calibration of the chromatograph was done with the Seven Anion Standard solution provided by Dionex. For IC analyses each filter sample was extracted with 5 mL of deionized water by sonication for at least fifteen minutes. The extracted samples were analyzed three times with a new background reading taken between the samples.

The results are shown in Table 2. The concentrations of ions present in coal and wood smoke displayed in the table are typical. As expected, coal showed the presence of more mineralogical components such as chloride and phosphate, as well as higher abundance of sulfur in the form of sulfate. Wood smoke contained increased amounts of nitrogen in the form of nitrate.

a.)

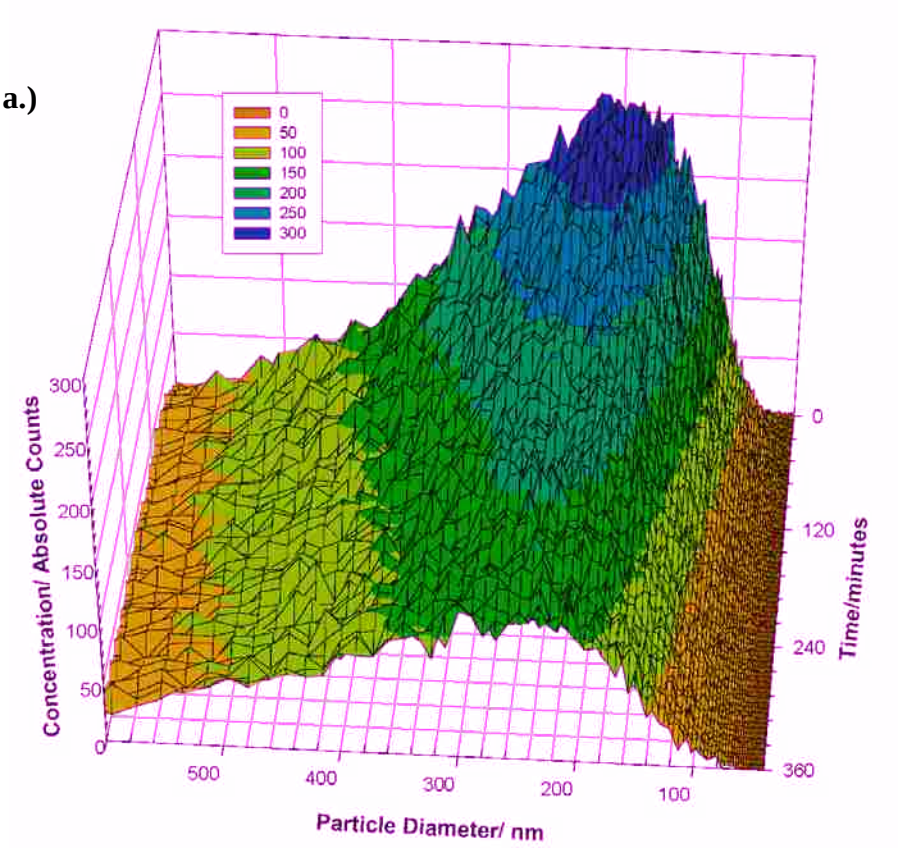

b.)

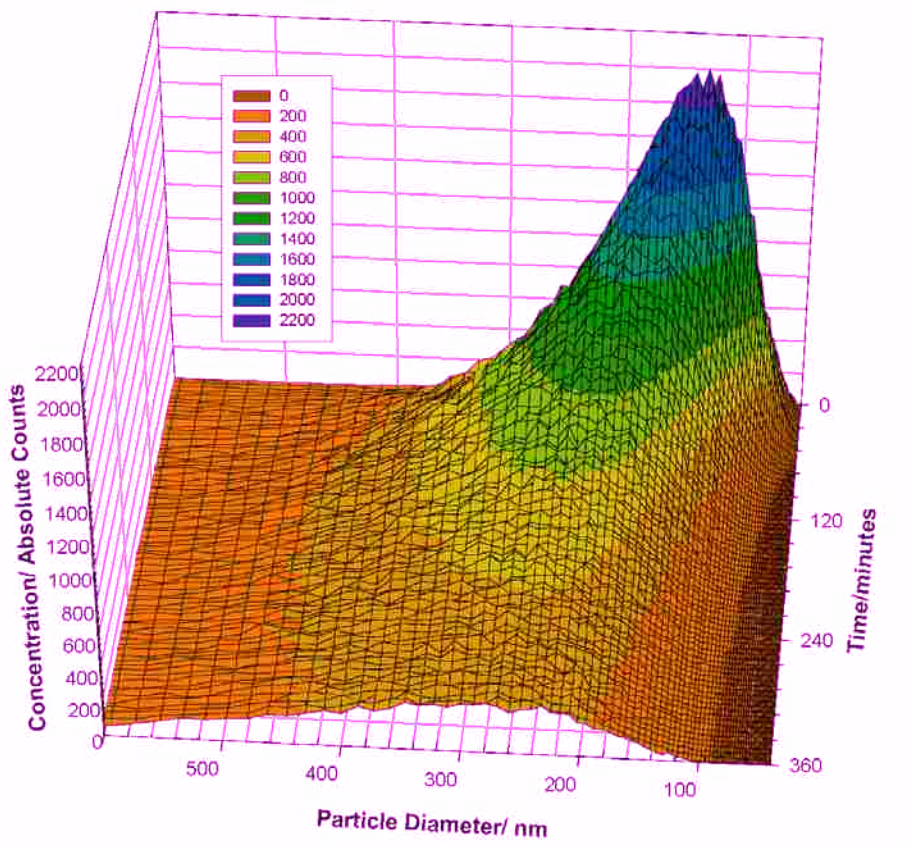

Figure 7. Aerodynamic diameter distribution of particles of a) coal smoke and b) photochemically aged wood smoke. Raw counts of particles according to their aerodynamic diameter with relation to time. Fresh coal smoke is mostly particles around 200 nm in diameter that later grow to 240-250 nm. Photochemically aged wood smoke particles begin prevalently at 130-140 nm and grow to 260-280 nm.

	Aged Wood Smoke	***Coal Smoke***
Cl^-	0.00±0.01%	0.42±0.01%
NO_2^-	0.03±0.00%	0.24±0.01%
NO_3^-	7.01±0.9%	0.52±0.01%
PO_4^{3-}	0.00±0.01%	0.92±0.4%
SO_4^{2-}	1.16±0.01%	1.70±0.01%

Table 2. Results of ion chromatographic anion analysis of aged wood and coal particles collected with 0.4 μm PTFE filters. Concentrations are given as the mass percentage of the total weight of the collected PM. Uncertainty is given as absolute error in the percentage.

X-ray Fluorescence analysis (XRF) was performed with a PANalytical Epsilon 5 XRF analyzer with a Gadolinium (Ga) anode as a source of X-rays and a solid state Germanium x-ray detector. Instrument calibration and sample analysis was performed by Desert Research Institute (DRI, NV). Table 3 shows the mass percent of the elements. As expected, sulfur was more abundant in coal smoke PM. Consistent with potassium being a biomass marker, potassium was the most prevalent element in the photochemically aged wood smoke PM.. The coal smoke PM also had a larger concentration of Pb, Cr and Hg relative to the photochemically aged wood smoke PM. Chloride content of coal ash found by XRF analysis was identical to that found via IC. A small concentration of iron was also observed in coal ash, most likely originating from pyrites, commonly present in coals. Only 28% of sulfur was detected as sulfate in coal and wood PM. Low sulfate yields may be attributed to formation of organic sulfur compounds as the result of incomplete combustion. Ultra-fine coal ash PM (<0.5μm diameter) is known to contain a measurable amount of thiophenic compounds which are stable at temperatures over 900°C in air.[47-49] Inorganic sulfides are also found as a byproduct of an incomplete combustion of coal even at temperatures as high as 1370°C in excess oxygen. Additionally, sulfites may have been produced which would further contribute to the reconciliation of sulfur balance.[48] Unfortunately, only sulfate was quantified and the presence of other forms of sulfur must be done by inference.

	Aged Wood Smoke	***Coal Smoke***
K	8.39±0.04%	0.24±0.03%
S	1.36±0.11%	2.01±0.15%
Cl	.027±0.03%	0.42±0.04%
Zn	0.34±0.02%	0.35±0.02%
Fe	0.00±0.04%	0.14±0.06%
Ca	0.25±0.03%	0.00±0.04%
Pb	0.00±0.04%	0.06±0.06%

Table 3. Results of X-ray fluorescence elemental analysis for aged wood smoke PM and coal smoke PM. Concentration of elements expressed in mass percentage of the collected PM. Uncertainty is given as absolute error in the percentage.

2.6 Stability of Conditions During an Exposure Experiment

Figure 8 shows the conditions (both gas and PM) during a typical exposure experiment. The presence of subjects inside the exposure room increased the PM loss rate. Because of the delay between the concentration change and the instrument response, PM was delivered into the exposure room at 15-20 minute intervals. This allowed regulating the exposure conditions without delivering excessive PM. Such oscillations in PM delivery resulted in the sinusoidal-like graph. In the representative conditions shown in Figure 8, the average concentration throughout the experiment was 190.7±20.5 $\mu g/m^3$ (standard deviation), close to the goal of 175 $\mu g/m^3$.

2.7 Conclusion

A chamber for human subject exposure experiments was designed and constructed. The design allows for the pretreatment of the particulate matter as well as for real-time control and monitoring of the conditions inside both the bag and the exposure room. Particulate matter used in the experiments was chemically and morphologically characterized. The design of the two-stage human exposure chamber presented here offers several distinct advantages. First, the generation and optional pretreatment of the particulate matter happens in a volume separated from the actual human exposure chamber. This allows for close monitoring and control of the PM and gas concentrations *before* the exposure. Second, the large panel of UV and black lamps directly above the first stage of the chamber provides the option of photochemically aging the PM so as to

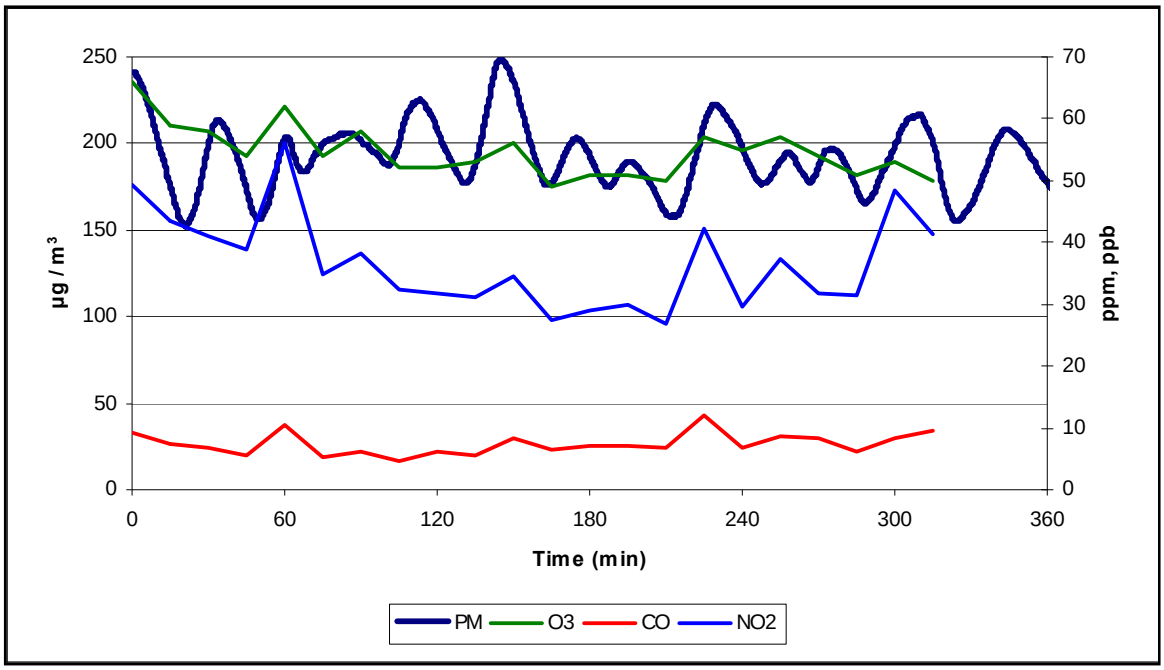

Figure 8. Gas and PM concentrations during a typical human exposure experiment. The average values of concentrations of gases and PM were held under regulatory standards and within experimental protocols. PM is reported in µg/m^3, CO is reported in ppm; O_3 and NO_2 in ppb.

mimic actual daytime conditions. Third, the construction of the exposure chamber allows interfacing with a wide range of monitoring and analyzing instruments, as well as the collection of PM for chemical and elemental analysis.

Chapter 3. Salt Lake City Study of Inversion Episodes during January and February of 2009

3.1 Introduction

Under the Clean Air Amendments of 1992, two regions in the State of Utah, Salt Lake Valley and Utah Valley, are in violation of the National Ambient Air Quality Standard for PM10. Both valleys are susceptible to strong inversions that can persist for weeks at a time. The strong inversions coupled with the metropolitan nature of this region contribute to its violation of the National Ambient Air Quality Standards for PM during the winter.

The Hawthorne Elementary School located in Salt Lake City, Utah has been designated as one of 55 proposed urban, long-term, nationwide multi-pollutant NCore sites. The NCore network is designed to enhance existing monitoring capabilities in an effort to produce an integrated multi-pollutant approach to air quality monitoring. In addition to collecting information on critical pollutants, NO_x, O_3, CO and PM, emphasis has been placed on measuring non-criteria pollutants, specifically NH_3 and HNO_3. These species are measured in an effort to improve emission control strategies as well as to obtain more complete information for scientific, public health and ecosystem assessments.

Previous air sampling campaigns have shown that a major component of the PM in Salt Lake Valley and Utah Valley is ammonium nitrate (NH_4NO_3). Ammonium nitrate is primarily formed from gas phase ammonia and nitric acid via reaction 1.:

$$NH_3(g) + HNO_3(g) \leftrightarrow NH_4NO_3\ (s) \qquad (1)$$

Ammonium nitrate assists in formation of particles of the appropriate size to scatter visible light which reduce visibility. One of the goals of this study is to identify the limiting reagent in the formation of ammonium nitrate PM in Salt Lake Valley.

This study presents the results of an air sampling campaign conducted from January 1, 2009 through February 25, 2009 at the Hawthorne Elementary School. During this time the Salt Lake Valley experienced prolonged episodes of inversions. A deep inversion occurred during the first half of this study with $PM_{2.5}$ concentrations as high as 125 μg/m3. The last half of this study was conducted during a moderately strong inversion with $PM_{2.5}$ concentration as high as 50 $\mu g/m^3$.

3.2 Method

One-hour averaged concentrations of PM_{10}, $PM_{2.5}$, NOx, O_3, CO, and NH_3 were measured. Particulate and gas phase nitrate, nitrite and sulfate were also measured. The PM size distribution (25-0.2 μm diameter) was also measured over a 15 hour period.

A URG-9000C Ambient Ion Monitor (AIM) provided one-hour averaged measurements of particulate and gas phase nitrate, nitrite, and sulfate in $PM_{2.5}$. The instrument draws in air at a rate of 3 lpm through a $PM_{2.5}$ sharp-cut cyclone filter. The air is passed through a liquid diffusion denuder where gases are removed by reaction with a dilute aqueous solution of H_2O_2 (0.003% in water). The gas phase is collected for one-hour and then analyzed with ion chromatography (Dionex ICS-1000). The air stream then enters an aerosol super-saturation chamber that enhances particle growth. An inertial particle separator collects and dissolves these particles in deionized water and

injects them into the ion chromatograph for analysis. The lower limit of detection for both particle and gas phase ions is species dependent and approximately 0.05 $\mu g/m^3$. The AIM instrument was calibrated according to the user manual instructions every two weeks with the seven anion standard purchased from Dionex (part number 56933). The denuder membrane was changed every four weeks.

To avoid sampling artifacts as well as weather interferences, sampling with the AIM was done through a manifold. The manifold was constructed from an 8 foot (2.44 meter) long PVC pipe with 6 inch (15.2 cm) diameter. A high volume air pump was connected to the air pipe and was set so that the air velocity inside the pipe was no more than 5 mph (8 km/h). A weather cap was attached to the top of the manifold to avoid ingestion of precipitation and large objects. The sampling manifold was raised at least 4 ft (1.2 m) over the roof of the sampling trailer and at least 2 feet above the closest sampling intake of other instruments.

Data on NO, NO_2, NOx, CO, NH_3, and O_3 concentrations were collected and reported by the Utah State Department of air quality.

3.3 PM Results and Discussion

Two distinct, persistent inversions occurred during the study. The first inversion began on January 14th and continued through January 24th. The second inversion period occurred from January 29th to February 6th. Both inversions were broken by a low-pressure airmass. On January 24th it brought 2.8 inches of snow along with approximately 1 inch of water. A sharp temperature increase (~5.6 °C) was observed on

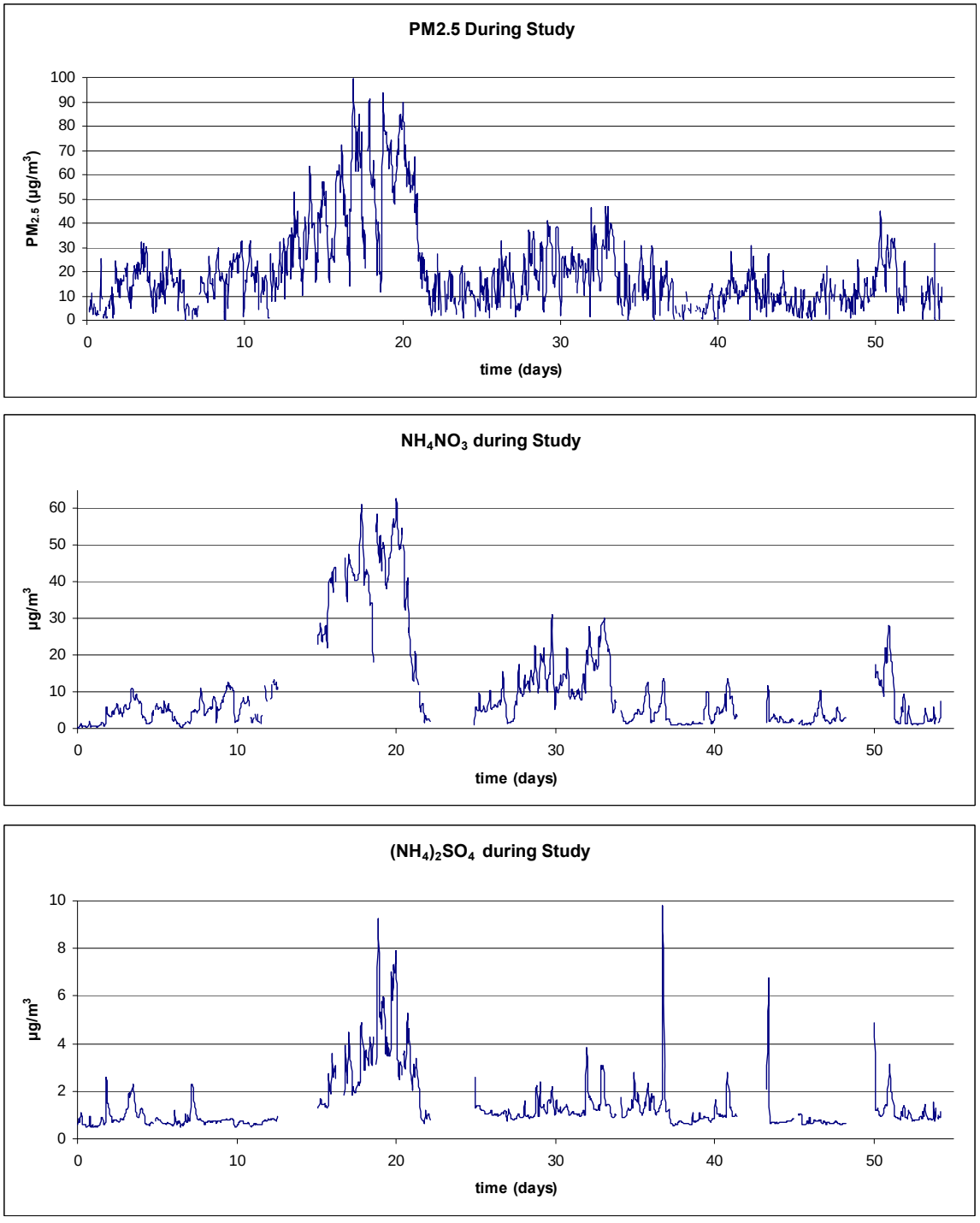

Figure 9. Plot of ammonium nitrate and ammonium sulfate along with the recorded $PM_{2.5}$ for the duration of the study.

February 6th. Both episodes were broken by an increase in wind speed (from ~3 mph to above 7 mph) and change of direction from north during the inversion to south at the end. Several other inversions lasting between 2 and 3 days were observed during the study, but none were as intense and persistent as the two mentioned above.

Figure 9 shows total $PM_{2.5}$ (non-volatile plus semi-volatile) plotted along with of particulate nitrate and sulfate expressed as their respective ammonium salts. A high concentration of NH_3 prevailed during the sampling campaign and therefore it is logical to assume that nitrate and sulfate are predominately in the form of their ammonium salts.

Diurnal variation in $PM_{2.5}$ was observed in the ammonium nitrate data. The strong correlation between the two (see Figure 10) suggests that a significant portion of the $PM_{2.5}$ is ammonium nitrate. The correlation between $PM_{2.5}$ and nitrate was more pronounced during inversions, when the formation of ammonium nitrate aided in secondary PM formation. The correlation was less pronounced during the non-inversion days.

The mass fraction of ammonium nitrate in $PM_{2.5}$ differed between the inversion periods and the less polluted days. PM during the major inversions contained between 70 and 80% ammonium nitrate whereas on days outside the major inversion periods ammonium nitrate was 40 to 50% of the $PM_{2.5}$ mass.

The mass fraction of ammonium sulfate also increased during the two major inversion periods when compared to the non-inversion days. A 8-10 mass percent ammonium sulfate of total PM was much lower than the mass percent of ammonium nitrate. However, sulfate and $PM_{2.5}$ were only moderately correlated. Even though most

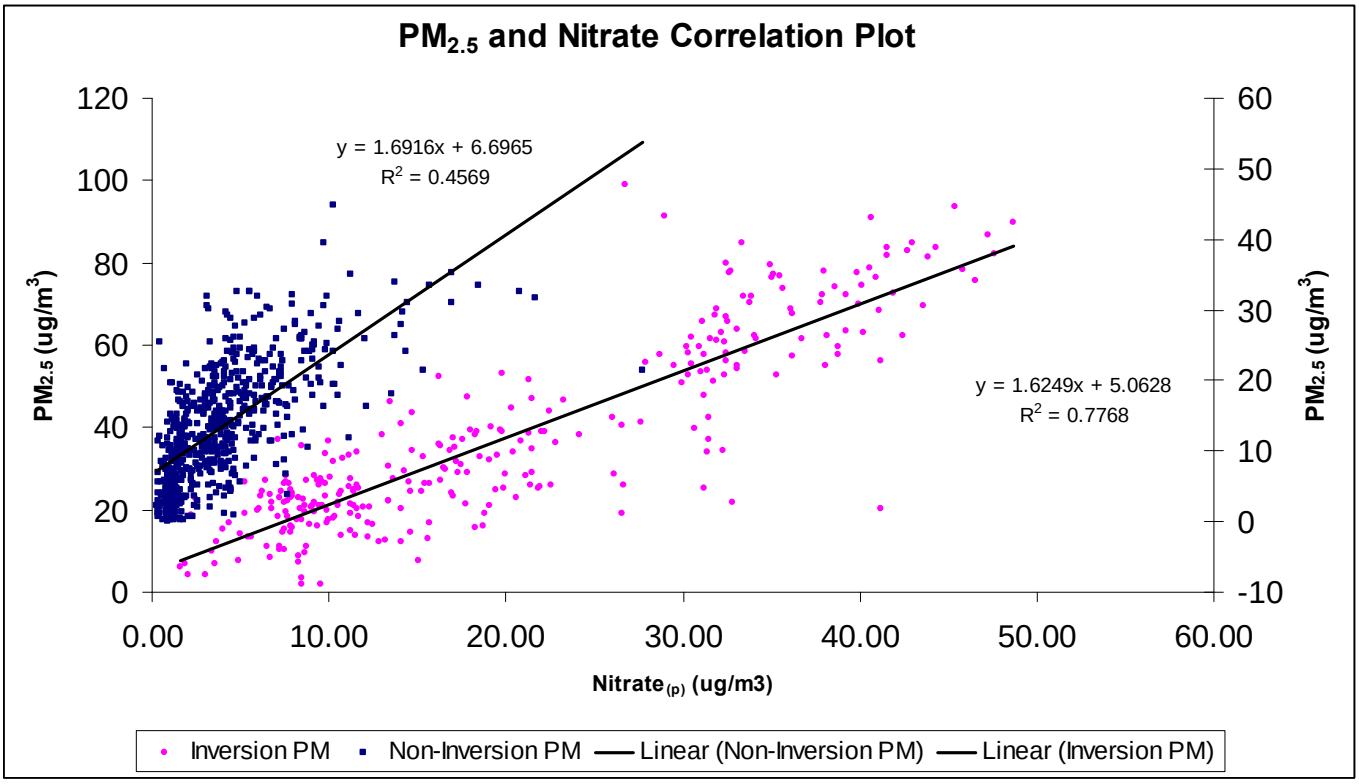

Figure 10. Correlation of $PM_{2.5}$ and particulate nitrate. The concentration of $PM_{2.5}$ is clearly correlated with the increase in particulate nitrate.

of the sulfate was in the particle phase, the primary source must not be associated with the major PM source. Total elemental sulfur was also not correlated with CO, a marker for primary emission sources (predominantly mobile sources).

Particulate nitrite had a very strong diurnal variation as a mass fraction of total $PM_{2.5}$: 6-8% during day and 10-40% at night. Such variation in mass fraction was due to nighttime increase, beginning around 6pm to nearly 6am, augmented by the overall decrease in ambient $PM_{2.5}$. During the inversion of Jan 29th to Feb 6th, nighttime nitrite rose from 4 $\mu g/m^3$ to nearly 7 $\mu g/m^3$ while $PM_{2.5}$ concentration declined from 60–70 $\mu g/m^3$ to 15 $\mu g/m^3$. This pattern is caused by nighttime accumulation of ambient nitrite from primary emission sources and lack of solar radiation initiated oxidative chemistry.

3.4 Gas Phase Results and Discussion

Baseline CO and NO_x increased during the two major inversions. CO was the dominant gas, followed by NO_x and ozone. All of the monitored gas species had a very strong diurnal variation.

Throughout the study, CO spiked during morning and afternoon commute hours and was elevated during evenings and nights, while morning CO peaks decreased during weekends and holidays and evening peaks showed slight decreases during weekends.

Figure 11 shows the diurnal variation of gasses, specifically the interrelationship between ozone, NO, and NO_2. The NO_2/NO ratio fluctuated from 1:1 during morning hours to 1:4 during evenings spikes. Such pattern is explained by the continued

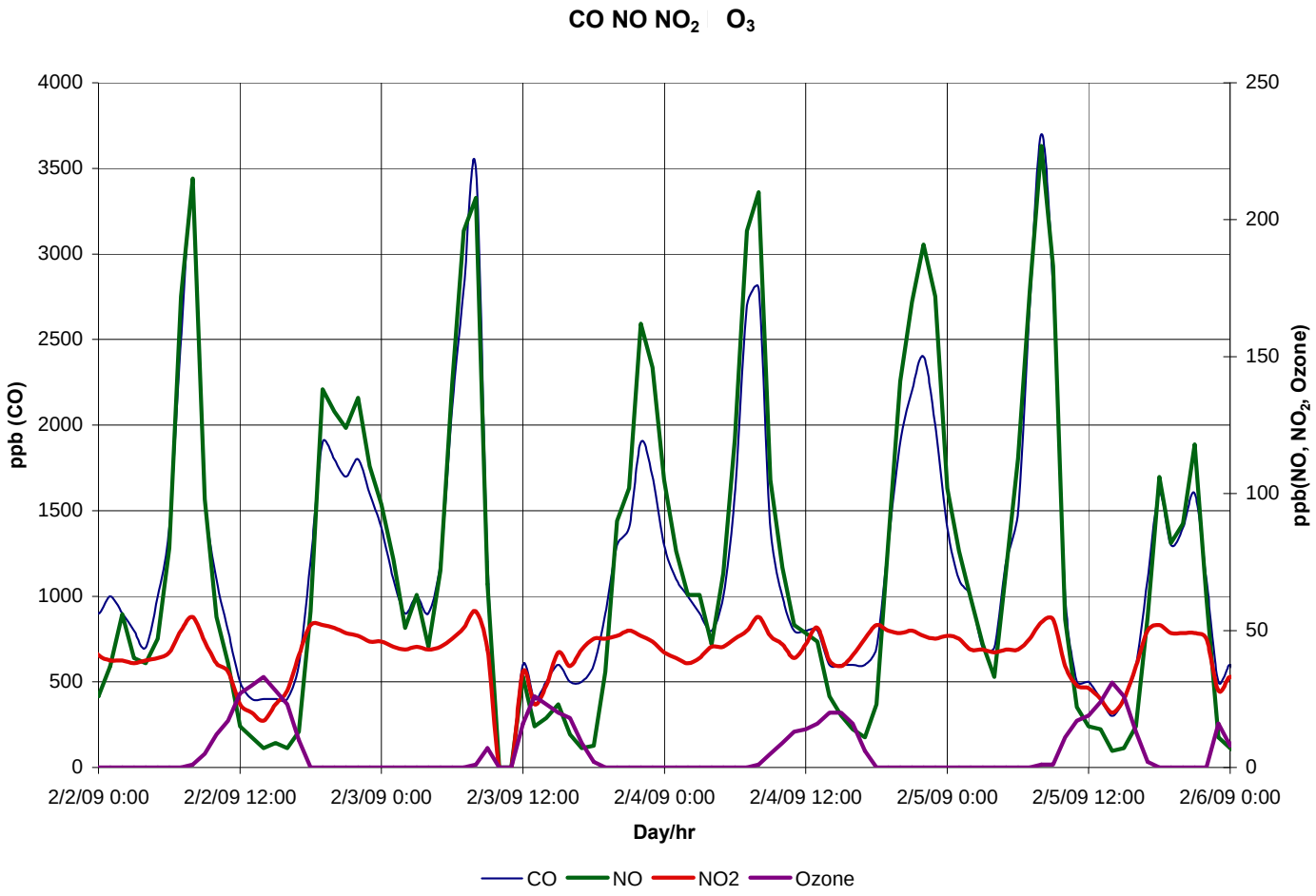

Figure 11. Diurnal Variation of CO, NO, NO_2, and O_3. Drops in NO_x concentrations are accompanied by increases in daytime ozone formation. NO/NO_2 composition of NO_x varies between daytime and nighttime.

NO emission from the primary sources coupled with the lack of photochemical oxidation to NO_2 and subsequent conversion to HNO_3 via reaction with OH radical.

The correlation between NO_x and CO is illustrated in Figure 12. NO_x composition varied depending on time of day. CO and NO_x were nearly linearly correlated throughout the study R^2=0.93. However, the slope of the correlation decreases at higher concentrations of CO (beginning at approximately 2000 ppb). The decreased correlation slope was observed during the peaks of the two major inversion periods.

Figure 13 shows the concentrations of gaseous ammonia and nitric acid. The concentration of ammonia always exceeded that of nitric acid by at least one order of magnitude.

Outside the major inversions, the concentration of nitric acid was ~0.3 ppb while during the inversion time it elevated to approximately 0.55 ppb. Although the concentration of ammonia fluctuated during the study, it was always at least an order of magnitude larger than nitric acid. Such conditions result in a conclusion that most of the nitric acid exists in particles as ammonium nitrate.

Assuming a pure ammonium nitrate particle, the calculated dissociation constant for NH_4NO_3 at 273 K and low relative humidity is 21 ppb^2, calculated using the Mozurkewich method.[50] The dissociation constant for ammonium nitrate, calculated from using the experimental data in this study, was between 5 and 10 ppb^2 during the strong inversion periods and below 3 ppb^2 during the non-inversion days. The difference in the calculated and measured dissociation constants is complicated due to the impure nature of the PM. During the non-inversion days approximately 40% of the mass of the PM is in

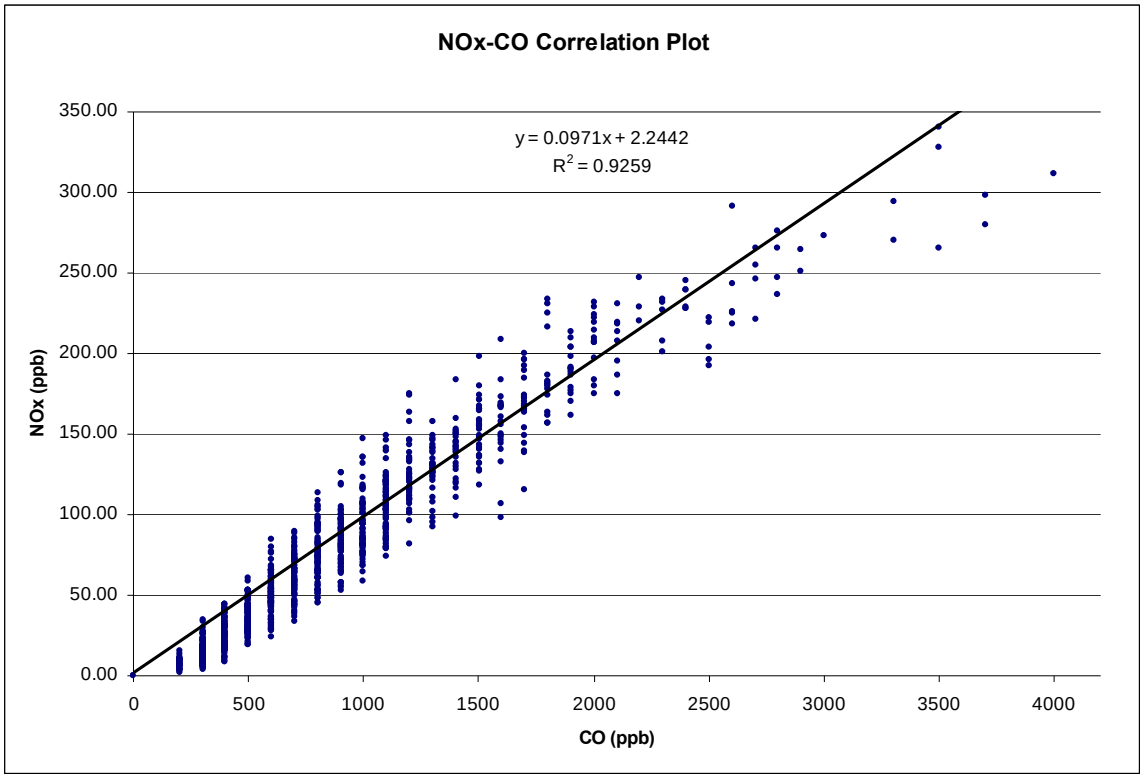

Figure 12. Correlation plot of NOx and CO. The strong correlation indicates a connection of CO and NO_x sources.

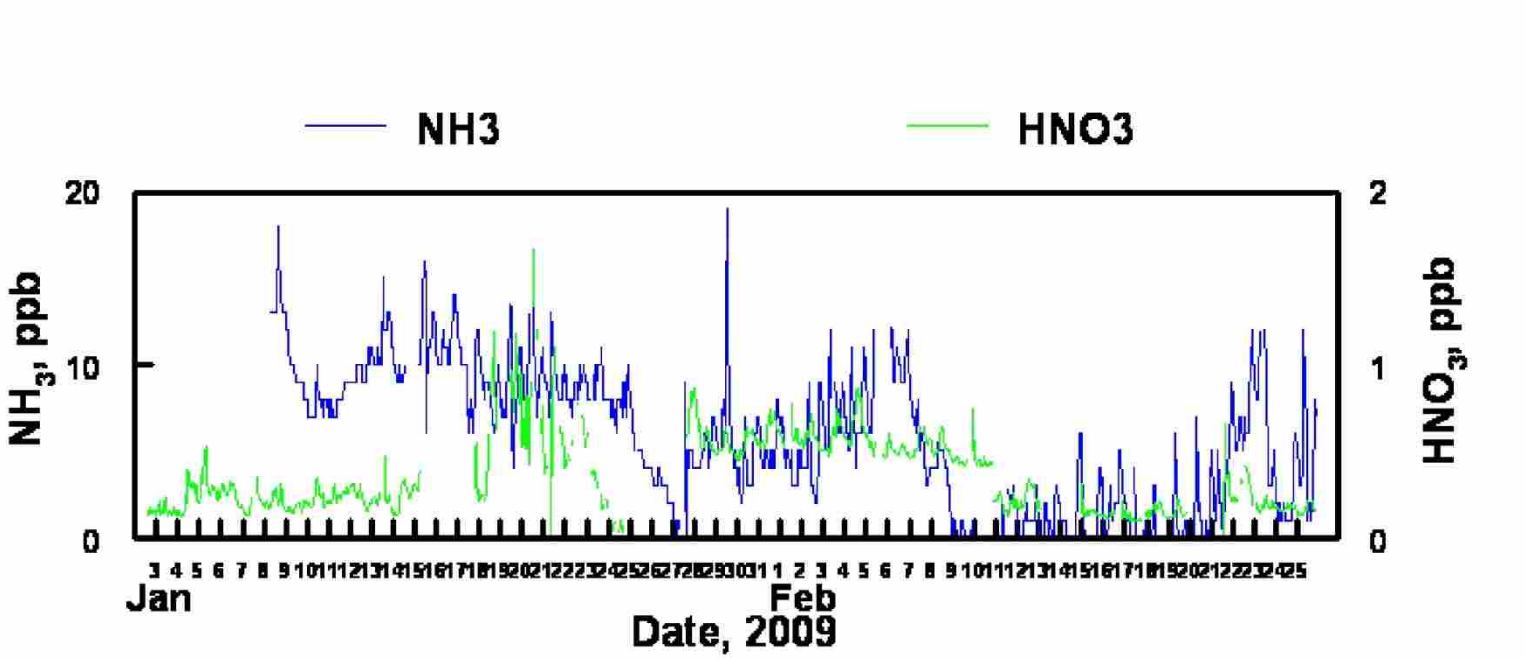

Figure 13. Gas phase concentrations of ammonia and nitric acid.

the form of ammonium nitrate. Consequently, it is expected that the measured dissociation constant will be smaller than the calculated value. Increased mass fraction of ammonium nitrate in PM during inversions (up to 80%) can be the responsible for the increase of the NH_4NO_3 dissociation constant for those days.

During the study, ozone peaked to 45 ppb, well within EPA regulations. The highest ozone concentrations did not occur during the two major inversions, but peaked between inversions. The diurnal variation of ozone was characterized by a sharp increase in ozone concentration beginning approximately at 7 a.m., peaking at about 2 p.m., followed by a sharp decline below the limit of detection of the instrument in the next four to five hours.

Figure 14 displays the relationship between ozone and NO_2, illustrating the inverse relationship, suggesting ozone scrubbing by NO. The sharp downward trend in the O_3/NO_2 relationship suggests an oxidant limited airmass. This conclusion is further strengthened by Figure 15, showing NO_2 plotted against NO_x. Upwards of 90% of NO_x is NO_2 at concentrations below 50 ppb. The linearity and density of the data deteriorates at concentrations of NO_x above 50 ppb. At 100 ppb of NO_x and higher, the relative NO_2 concentrations were remained in the range of 40 – 60 ppb, indicative of the lack of oxidant species necessary to convert NO to NO_2. This deficiency can be explained by low VOC concentrations. Although VOC's were not measured directly it can be assumed that they were scarce due to the decrease of the ozone concentration with the increase of NO_x, signifying the lack of RO_2 radicals and the use of ozone to convert NO to NO_2.

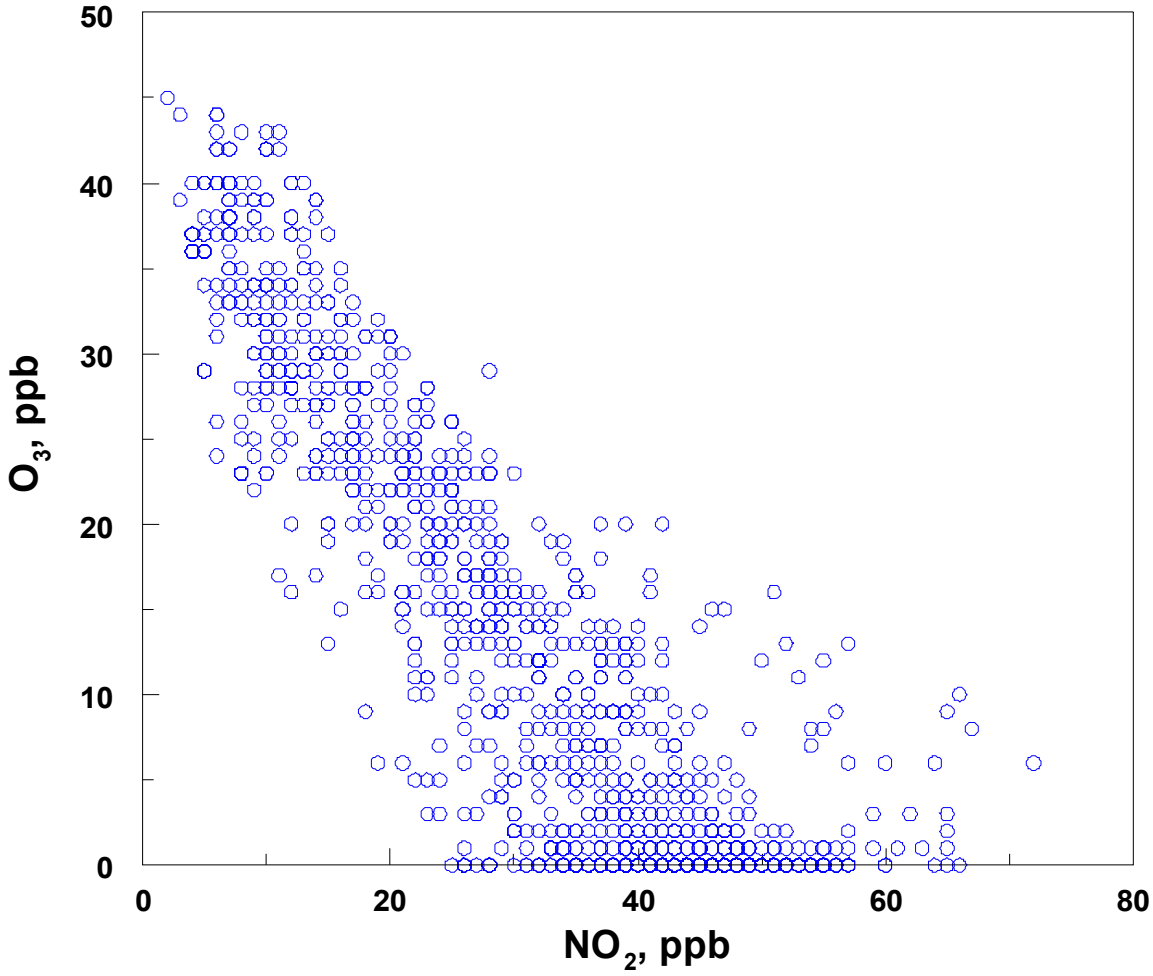

Figure 14. Correlation plot of ozone and NOx, both expressed in units of ppb. The lack of ozone at higher NOx concentrations signifies the lack of oxidative species in the system to convert NO to NO2.

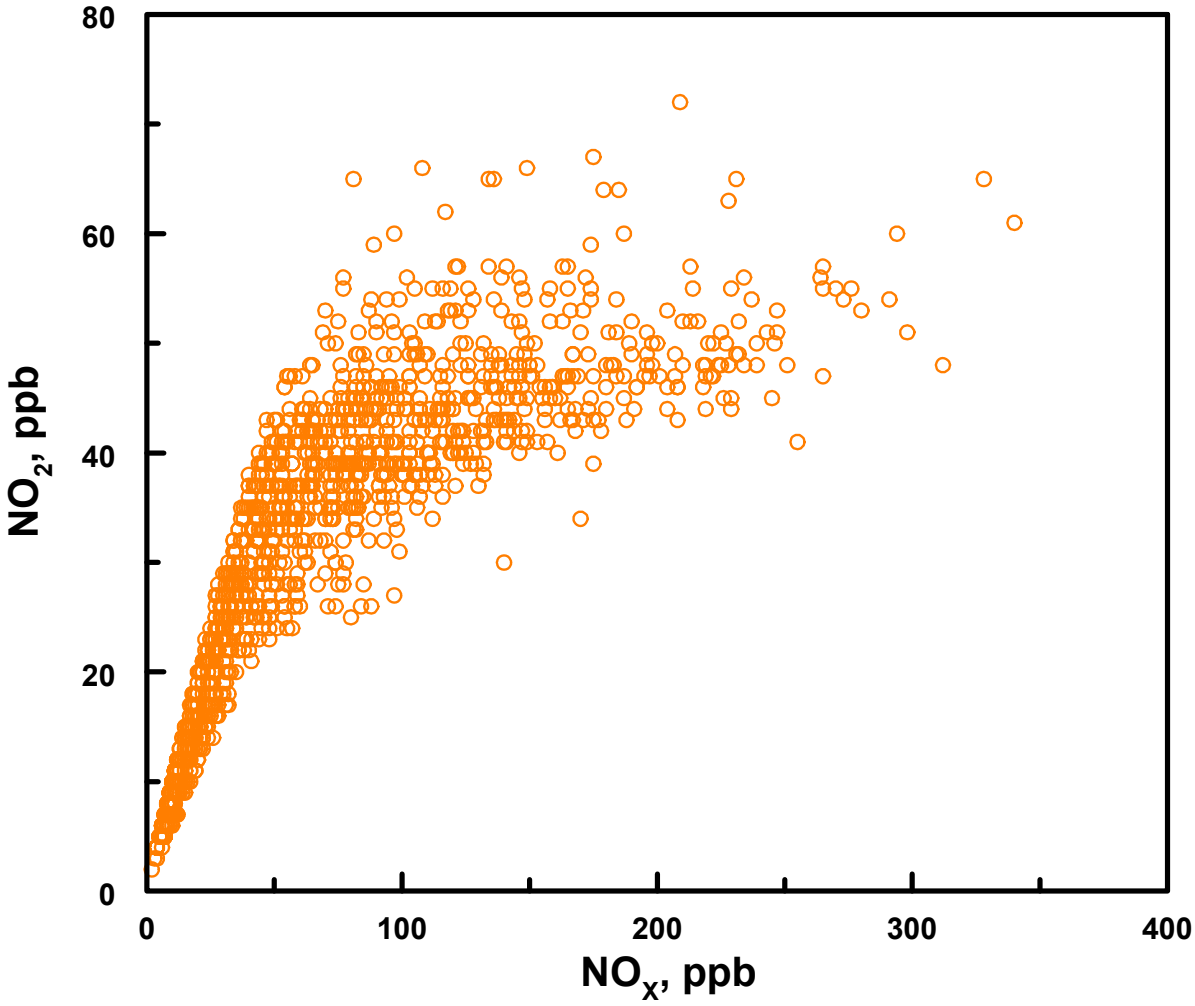

Figure 15. NO_2/NO_x correlation plot. Decreasing contribution of NO_2 in growing NO_x is indicative of the limited supply of oxidizing species.

underestimated. Some increased activity of the oxidative processes involving sulfur species was observed during the afternoons across the whole study that were characterized by high SO_2 concentration spikes when compared to the concentrations of SO_4^{2-}. A corresponding increase in SO_4^{2-} was also observed during those periods. Throughout the duration of the study, however, the concentration of particulate sulfate never exceeded ~0.6 $\mu g/m^3$ except during the afternoon spikes, reaching as high as 6.7 $\mu g/m^3$ during the major inversion times but no higher than 2.7 $\mu g/m^3$ during the non-inversion days. The concentration of SO_2 was nearly identical to that of SO_4^{2-} at all times except for the afternoon spikes reaching as high as 15-20 $\mu g/m^{3.}$

Figure 16 shows that the missing mass of total PM was not as large during the major inversion periods as during non-inversion days. Because direct measurements of elemental and organic carbon were not performed during the study, carbon was approximated as the missing mass. Organic and elemental carbon contribution was calculated by subtracting ammonium nitrate, ammonium sulfate, ammonium nitrite and ammonium chloride from the mass of $PM_{2.5}$. The contribution of missing mass was less pronounced during the inversion days (~40-50%) and significant during the non-inversion days (80-90%).

3.5 Conclusions

Ammonium nitrate constitutes 40-50% of the total $PM_{2.5}$ and up to 80% during strong inversions. Formation of ammonium nitrate is nitrate limited, with a large excess of ammonia present. Sulfates and nitrites together constitute 15% - 20% of the total $PM_{2.5}$ and are not as significant as ammonium nitrate. Ozone levels throughout the study

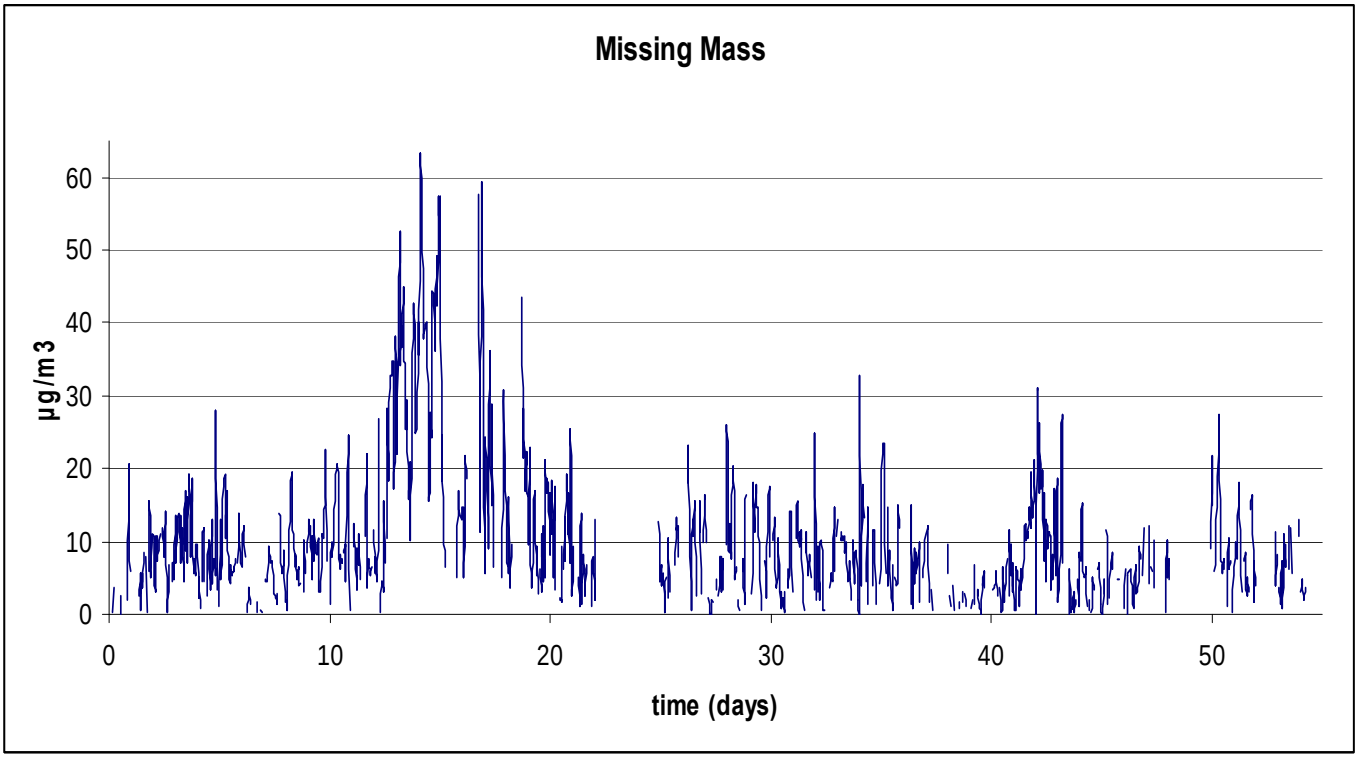

Figure 16. Organic and elemental carbon contributions are calculated as the missing mass throughout the study.

remained well below EPA limits. Overall, the lower boundary layer in the Salt Lake valley was found to be oxidant and VOC deficient.

Because ozone levels during the study remained within EPA standards, the most effective way of reducing contributions of ammonium nitrate to secondary particle formation during the inversion periods is to decrease NO_x emissions.

References:

1. Conner, W. D.; Bennett, R. L.; Weathers, W. S.; Wilson, W. E., Particulate Characteristics and Visual Effects of the Atmosphere at Research-Triangle-Park. *J. Air Waste Manage. Assoc.* **1991,** *41* (2), 154-160.
2. Watson, J. G.; Thurston, G.; Frank, N.; Lodge, J. P.; Wiener, R. W.; McElroy, F. F.; Kleinman, M. T.; Mueller, P. K.; Schmidt, A. C.; Lipfert, F. W.; Thompson, R. J.; Dasgupta, P. K.; Marrack, D.; Michaels, R. A.; Moore, T.; Penkala, S.; Tombach, I.; Vestman, L.; Hauser, T.; Chow, J. C., 1995 Critical-Review Discussion - Measurement Methods to Determine Compliance with Ambient Air-Quality Standards for Suspended Particles. *J. Air Waste Manage. Assoc.* **1995,** *45* (9), 666-684.
3. Whitby, K. T.; Sverdrup, G. M., California Aerosols: Their Physical and Chemical Characteristics. *Adv. Environ. Sci. Technol.* **1980,** *8*, 477-525.
4. Schmidt, D. S.; Schmidt, R. A.; Dent, J. D., Electrostatic force on saltating sand. *J. Geophys. Res.-Atmos.* **1998,** *103* (D8), 8997-9001.
5. Chiapello, I.; Bergametti, G.; Chatenet, B.; Bousquet, P.; Dulac, F.; Soares, E. S., Origins of African dust transported over the northeastern tropical Atlantic. *J. Geophys. Res.-Atmos.* **1997,** *102* (D12), 13701-13709.
6. Moulin, C.; Lambert, C. E.; Dulac, F.; Dayan, U., Control of atmospheric export of dust from North Africa by the North Atlantic oscillation. *Nature* **1997,** *387* (6634), 691-694.
7. Prospero, J. M.; Glaccum, R. A.; Nees, R. T., Atmospheric Transport of Soil Dust from Africa to South-America. *Nature* **1981,** *289* (5798), 570-572.
8. Prospero, J. M.; Nees, R. T., Impact of the North African Drought and El-Nino on Mineral Dust in the Barbados Trade Winds. *Nature* **1986,** *320* (6064), 735-738.
9. Pope, C. A.; Dockery, D. W., Health effects of fine particulate air pollution: Lines that connect. *J. Air Waste Manage. Assoc.* **2006,** *56* (6), 709-742.
10. Benoit, N.; Peter, H. M. H.; Abderrahim, N., The Meuse Valley fog of 1930: An air pollution disaster. *The Lancet* **2001,** *357* (9257), 704.
11. Health, U. K. M. o., The Report of the Chief Medical Officer on the State of Public Health. **1953**.
12. Health, U. K. M. o., Mortality and Morbidity during the London Fog of December 1952. *Reports on Public Health and Medical Subjects* **1954,** *95*.
13. Dockery, D. W.; Pope, C. A.; Xu, X. P.; Spengler, J. D.; Ware, J. H.; Fay, M. E.; Ferris, B. G.; Speizer, F. E., An Association Between Air-Pollution and Mortality in 6 United-States Cities. *New England Journal of Medicine* **1993,** *329* (24), 1753-1759.
14. Pope, C. A., Respiratory Hospital Admissions Associated with PM-10 Pollution in Utah, Salt-Lake, and Cache Valleys. *Archives of Environmental Health* **1991,** *46* (2), 90-97.
15. Ransom, M. R.; Pope, C. A., Elementary-School Absences and PM(10) Pollution in Utah Valley. *Environ. Res.* **1992,** *58* (2), 204-219.
16. Ransom, M. R.; Pope, C. A., External Health Costs of a Steel Mill. *Contemp. Econ. Policy* **1995,** *13* (2), 86-97.
17. Gauderman, W. J.; Avol, E.; Gilliland, F.; Vora, H.; Thomas, D.; Berhane, K.; McConnell, R.; Kuenzli, N.; Lurmann, F.; Rappaport, E.; Margolis, H.; Bates, D.; Peters,

J., The Effect of Air Pollution on Lung Development from 10 to 18 Years of Age. *N Engl J Med* **2004,** *351* (11), 1057-1067.
18. Avol, E. L.; Gauderman, W. J.; Tan, S. M.; London, S. J.; Peters, J. M., Respiratory effects of relocating to areas of differing air pollution levels. *American Journal of Respiratory and Critical Care Medicine* **2001,** *164* (11), 2067-2072.
19. Tashkin, D. P.; Detels, R.; Simmons, M.; Liu, H. H.; Coulson, A. H.; Sayre, J.; Rokaw, S., The UCLA Population Studies of Chronic Obstructive Respiratory-Disease: Impact of Air-Pollution And Smoking on Annual Change in Forced Expiratory Volume in One-Second. *American Journal of Respiratory and Critical Care Medicine* **1994,** *149* (5), 1209-1217.
20. Abbey, D. E.; Hwang, B. L.; Burchette, R. J.; Vancuren, T.; Mills, P. K., Estimated Long-Term Ambient Concentrations of PM(10) and Developement of Respiratory Symptoms in a Nonsmoking Population. *Archives of Environmental Health* **1995,** *50* (2), 139-152.
21. Dockery, D. W.; Cunningham, J.; Damokosh, A. I.; Neas, L. M.; Spengler, J. D.; Koutrakis, P.; Ware, J. H.; Raizenne, M.; Speizer, F. E., Health effects of acid aerosols on North American children: Respiratory symptoms. *Environmental Health Perspectives* **1996,** *104* (5), 500-505.
22. Raizenne, M.; Neas, L. M.; Damokosh, A. I.; Dockery, D. W.; Spengler, J. D.; Koutrakis, P.; Ware, J. H.; Speizer, F. E., Health effects of acid aerosols on North American children: Pulmonary function. *Environmental Health Perspectives* **1996,** *104* (5), 506-514.
23. AckermannLiebrich, U.; Leuenberger, P.; Schwartz, J.; Schindler, C.; Monn, C.; Bolognini, C.; Bongard, J. P.; Brandli, O.; Domenighetti, G.; Elsasser, S.; Grize, L.; Karrer, W.; Keller, R.; KellerWossidlo, H.; Kunzli, N.; Martin, B. W.; Medici, T. C.; Perruchoud, A. P.; Schoni, M. H.; Tschopp, J. M.; Villiger, B.; Wuthrich, B.; Zellweger, J. P.; Zemp, E., Lung function and long term exposure to air pollutants in Switzerland. *American Journal of Respiratory and Critical Care Medicine* **1997,** *155* (1), 122-129.
24. van Eeden, S. F.; Yeung, A.; Quinlam, K.; Hogg, J. C., Systemic Response to Ambient Particulate Matter: Relevance to Chronic Obstructive Pulmonary Disease. *Proc Am Thorac Soc* **2005,** *2* (1), 61-67.
25. Sorensen, M.; Daneshvar, B.; Hansen, M.; Dragsted, L. O.; Hertel, O.; Knudsen, L.; Loft, S., Personal PM2.5 Exposure and Markers of Oxidative Stress in Blood. *Environmental Health Perspectives* **2003,** *111* (2), 161-165.
26. Seaton, A.; Macnee, W.; Donaldson, K.; Godden, D., Particulate Air Pollution And Acute Health-Effects. *Lancet* **1995,** *345* (8943), 176-178.
27. Schwartz, J., Air pollution and blood markers of cardiovascular risk. *Environmental Health Perspectives* **2001,** *109*, 405-409.
28. Souza, M. B.; Saldiva, P. H. N.; Pope, C. A.; Capelozzi, V. L., Respiratory changes due to long-term exposure to urban levels of air pollution - A histopathologic study in humans. *Chest* **1998,** *113* (5), 1312-1318.
29. Nolan, J.; Batin, P. D.; Andrews, R.; Lindsay, S. J.; Brooksby, P.; Mullen, M.; Baig, W.; Flapan, A. D.; Cowley, A.; Prescott, R. J.; Neilson, J. M. M.; Fox, K. A. A., Prospective Study of Heart Rate Variability and Mortality in Chronic Heart Failure : Results of the United Kingdom Heart Failure Evaluation and Assessment of Risk Trial (UK-Heart). *Circulation* **1998,** *98* (15), 1510-1516.

30. La Rovere, M. T.; Pinna, G. D.; Maestri, R.; Mortara, A.; Capomolla, S.; Febo, O.; Ferrari, R.; Franchini, M.; Gnemmi, M.; Opasich, C.; Riccardi, P. G.; Traversi, E.; Cobelli, F., Short-Term Heart Rate Variability Strongly Predicts Sudden Cardiac Death in Chronic Heart Failure Patients. *Circulation* **2003,** *107* (4), 565-570.
31. Watkinson, W. P.; Campen, M. J.; Nolan, J. P.; Costa, D. L., Cardiovascular and Systemic Responses to Inhaled Pollutants in Rodents: Effects of Ozone and Particulate Matter. *Environmental Health Perspectives* **2001,** *109*, 539-546.
32. Wellenius, G. A.; Saldiva, P. H. N.; Batalha, J. R. F.; Krishna Murthy, G. G.; Coull, B. A.; Verrier, R. L.; Godleski, J. J., Electrocardiographic Changes during Exposure to Residual Oil Fly Ash (ROFA) Particles in a Rat Model of Myocardial Infarction. *Toxicol. Sci.* **2002,** *66* (2), 327-335.
33. Wichers, L. B.; Nolan, J. P.; Winsett, D. W.; Ledbetter, A. D.; Kodavanti, U. P.; Schladweiler, M. C. J.; Costa, D. L.; Watkinson, W. P. In *Effects of instilled combustion-derived particles in spontaneously hypertensive rats. Part I: Cardiovascular responses*, Taylor & Francis Inc: 2004; pp 391-405.
34. Schwartz, J.; Park, S. K.; O'Neill, M. S.; Vokonas, P. S.; Sparrow, D.; Weiss, S.; Kelsey, K., Glutathione-S-transferase M1, obesity, statins, and autonomic effects of particles - Gene-by-drug-by-environment interaction. *American Journal of Respiratory and Critical Care Medicine* **2005,** *172* (12), 1529-1533.
35. Brook, R. D.; Brook, J. R.; Urch, B.; Vincent, R.; Rajagopalan, S.; Silverman, F., Inhalation of fine particulate air pollution and ozone causes acute arterial vasoconstriction in healthy adults. *Circulation* **2002,** *105* (13), 1534-1536.
36. NEMMAR, A.; VANBILLOEN, H.; HOYLAERTS, M. F.; HOET, P. H. M.; VERBRUGGEN, A.; NEMERY, B., Passage of Intratracheally Instilled Ultrafine Particles from the Lung into the Systemic Circulation in Hamster. *Am. J. Respir. Crit. Care Med.* **2001,** *164* (9), 1665-1668.
37. Nemmar, A.; Hoet, P. H. M.; Vanquickenborne, B.; Dinsdale, D.; Thomeer, M.; Hoylaerts, M. F.; Vanbilloen, H.; Mortelmans, L.; Nemery, B., Passage of Inhaled Particles Into the Blood Circulation in Humans. *Circulation* **2002,** *105* (4), 411-414.
38. Thomas, P. T.; Zelikoff, J. T., Air Pollutants: Modulators of PUlmonary Host Resistance Against Infection. *Air Pollution and Health* **1999**, 357-379.
39. Ghio, A. J.; Gilrey, J. G.; Roggli, V. L.; Richards, J. H.; McGee, J. K.; Carson, J. L.; Devlin, R. B.; Cascio, W. E., Diffuse Alveolar Damage after Exposure to an Oil Fly Ash. *Am. J. Respir. Crit. Care Med.* **2001,** *164* (8), 1514-1518.
40. *National Vital Statistics Reports* **2007,** *55* (19).
41. Chen, L. C.; Nadziejko, C., Effects of subchronic exposures to concentrated ambient particles (CAPs) in mice: V. CAPs exacerbate aortic plaque development in hyperlipidemic mice. *Inhal. Toxicol.* **2005,** *17* (4-5), 217-224.
42. Sun, Q. H.; Wang, A. X.; Jin, X. M.; Natanzon, A.; Duquaine, D.; Brook, R. D.; Aguinaldo, J. G. S.; Fayad, Z. A.; Fuster, V.; Lippmann, M.; Chen, L. C.; Rajagopalan, S., Long-term air pollution exposure and acceleration of atherosclerosis and vascular inflammation in an animal model. *JAMA-J. Am. Med. Assoc.* **2005,** *294* (23), 3003-3010.
43. Wellenius, G. A.; Coull, B. A.; Godleski, J. J.; Koutrakis, P.; Okabe, K.; Savage, S. T.; Lawrence, J. E.; Murthy, G. G. K.; Verrier, R. L., Inhalation of concentrated ambient air particles exacerbates myocardial ischemia in conscious dogs. *Environmental Health Perspectives* **2003,** *111* (4), 402-408.

44. Lundgren, L.; Skare, L.; Liden, C.; Tornling, G., Large organic aerosols in a dynamic and continuous whole-body exposure chamber tested on humans and on a heated mannequin. *Ann. Occup. Hyg.* **2006,** *50* (7), 705-715.
45. O'Shaughnessy, P. T.; Mehaffy, J.; Watt, J.; Sigurdarson, S.; Kline, J. N., Characterization of a hooded human exposure apparatus for inhalation of gases and aerosols. *J. Occup. Environ. Hyg.* **2004,** *1* (3), 161-166.
46. Sostrand, P.; Kongerud, J.; Eduard, W.; Nilsen, T.; Skogland, M.; Boe, J., A test chamber for experimental hydrogen fluoride exposure in humans. *Am. Ind. Hyg. Assoc. J.* **1997,** *58* (7), 521-525.
47. Calkins, W. H., INVESTIGATION OF ORGANIC SULFUR-CONTAINING STRUCTURES IN COAL BY FLASH PYROLYSIS EXPERIMENTS. *Energy Fuels* **1987,** *1* (1), 59-64.
48. Furuya, K.; Kato, Y.; Kikuchi, T.; Gohshi, Y., STATE ANALYSIS OF SULFUR IN COAL AND COAL FLY-ASH BY DOUBLE-CRYSTAL X-RAY-FLUORESCENCE SPECTROMETRY. *Mikrochim. Acta* **1983,** *2* (3-4), 263-270.
49. Linak, W. P.; Yoo, J. I.; Wasson, S. J.; Zhu, W.; Wendt, J. O. L.; Huggins, F. E.; Chen, Y.; Shah, N.; Huffman, G. P.; Gilmour, M. I., Ultrafine ash aerosols from coal combustion: Characterization and health effects. *Proc. Combust. Inst.* **2007,** *31*, 1929-1937.
50. Mozurkewich, M., The Dissociation Constant of Ammonium Nitrate and Its Dependence on Temperature, Relative Humidity, and Particle Size. *Atmospheric Environment Part a-General Topics* **1993,** *27* (2), 261-270.